Article (refereed) - postprint

Piao, Silong; Sitch, Stephen; Ciais, Philippe; Friedlingstein, Pierre; Peylin, Philippe; Wang, Xuhui; Ahlstrom, Anders; Anav, Alessandro; Canadell, Josep G.; Cong, Nan; Huntingford, Chris; Jung, Martin; Levis, Sam; Levy, Peter E.; Li, Junsheng; Lin, Xin; Lomas, Mark R.; Lu, Meng; Luo, Yiqi; Ma, Yuecun; Myneni, Ranga B.; Poulter, Ben; Sun, ZhenZhong; Wang, Tao; Viovy, Nicolas; Zaehle, Soenke; Zeng, Ning. 2013. **Evaluation of terrestrial carbon cycle models for their response to climate variability and to CO2 trends.** *Global Change Biology*, 19 (7). 2117-2132. https://doi.org/10.1111/gcb.12187

Evaluation of terrestrial carbon cycle models for their response to climate variability and to CO_2 trends

Shilong Piao[1,2], Stephen Sitch[3], Philippe Ciais[4], Pierre Friedlingstein[3], Philippe Peylin[4], Xuhui Wang[1], Anders Ahlström[5], Alessandro Anav[3], Josep G. Canadell[6], Chris Huntingford[7], Martin Jung[8], Sam Levis[9], Peter E. Levy[10], Junsheng Li[11], Xin Lin[11, 12], Mark R Lomas[13], Meng Lu[14], Yiqi Luo[15], Yuecun Ma[1], Ranga B. Myneni[16], Ben Poulter[4], ZhenZhong Sun[1], Tao Wang[4], Nicolas Viovy[4], Soenke Zaehle[8], Ning Zeng[17]

[1] Sino-French Institute for Earth System Science, College of Urban and Environmental Sciences, Peking University, Beijing 100871, China

[2] Institute of Tibetan Plateau Research, Chinese Academy of Sciences, Beijing 100085, China

[3] College of Engineering, Computing and Mathematics, University of Exeter, Exeter EX4 4QF, UK

[4] Laboratoire des Sciences du Climat et de l'Environnement, CEA CNRS UVSQ, 91191 Gif-sur-Yvette, France

[5] Department of Earth and Ecosystem Sciences, Lund University, Sölvegatan 12, SE–223 62 Lund

[6] Global Carbon Project, Commonwealth Scientific and Industrial Research Organization Marine and Atmospheric Research, Canberra, Australia

[7] Centre for Ecology and Hydrology, Benson Lane, Wallingford OX10 8BB, UK

[8] Max Planck Institute for Biogeochemistry, P.O. Box 10 01 64, 07701 Jena, Germany

[9] National Center for Atmospheric Research, Boulder, Colorado, USA

[10] Centre for Ecology and Hydrology, Bush Estate, Penicuik, Midlothian EH26 0QB, UK

[11] State Key Laboratory of Environmental Criteria and Risk Assessment, Chinese Research Academy of Environmental Sciences, Beijing 100012, People's Republic of China

[12] College of Water Sciences, Beijing Normal University, Beijing 100875, People's Republic of China

[13] Department of Animal & Plant Sciences, University of Sheffield, Sheffield S10 2TN, UK

[14] Institute of Biodiversity Science, Fudan University, 220 Handan Road, Shanghai 200433,

China

[15] University of Oklahoma, Department of Botany and Microbiology, Norman, Oklahoma 73019 USA

[16] Department of Geography and Environment, Boston University, 675 Commonwealth Avenue, Boston, MA 02215, USA

[17] Department of Atmospheric and Oceanic Science, University of Maryland, College Park, MD 20740, USA

Running title: Evaluation of terrestrial carbon cycle models

Keywords: Carbon cycle; CO_2 fertilization; Precipitation sensitivity; Model evaluation; Temperature sensitivity

Revised Manuscript for *Global Change Biology*

Corresponding author*:* Shilong Piao (slpiao@pku.edu.cn)

Abstract

The purpose of this study is to evaluate 10 process-based terrestrial biosphere models that were used for the IPCC 5th Assessment Report. The simulated distribution of gross primary productivity (GPP) is compared with gridded estimates established from a data-driven model based upon flux-tower measurements by Jung et al. (2011) (JU11). The net primary productivity (NPP) apparent sensitivity to climate variability and atmospheric CO_2 trends is diagnosed from each model output, using statistical functions. The temperature sensitivity is compared against independent ecosystem field warming experiments results. The CO2 sensitivity of NPP is compared to the results from four Free Air CO_2 Enrichment (FACE) experiments. The simulated global net biome productivity (NBP) is compared with the residual land sink (RLS) of the global carbon budget from Friedlingstein et al. (2010) (FR10). We found that models produce a higher GPP (133±15 Pg C yr^{-1}) than JU11 (118±6 Pg C yr^{-1}). In response to rising atmospheric CO_2 concentration, modelled NPP increases on average by 16% (5-20%) per 100 ppm, a slightly larger apparent sensitivity of NPP to CO_2 than that measured at the FACE experiment locations (13 % per 100 ppm). Global NBP differs markedly among individual models, although the mean value of 2.0±0.8 Pg C yr^{-1} is remarkably close to the mean value of RLS (2.1±1.2 Pg C yr^{-1}). The interannual variability of modelled NBP is significantly correlated with that of RLS for the period 1980-2009. The average linear regression slope of global NBP vs. Mean Annual Temperature (MAT) across the 10 models is -3.0±1.5 Pg C yr^{-1} $^oC^{-1}$. Yet, 9 of 10 models overestimate the regression slope of NBP vs. precipitation, compared to the slope of the observed RLS vs. precipitation. With most models lacking processes that control GPP and NBP in addition to CO_2 and climate, such as N-deposition, forest regrowth, changes in the diffuse component of radiation, the agreement between modelled and observation-based GPP and NBP can be fortuitous. Carbon-nitrogen interactions (only separable in one model) significantly influence the simulated response of GPP and NBP to temperature and atmospheric CO_2 concentration, suggesting that nutrients limitations should be included in the next generation of terrestrial biosphere models.

1. Introduction

The human caused perturbation of the carbon cycle controls climate change, directly through emissions but also via climate feedbacks on natural carbon sources and sinks. The terrestrial carbon cycle has been modeled to be particularly sensitive to current and future climate and atmospheric CO_2 changes, but regional patterns and mechanisms of terrestrial carbon sources and sinks remain uncertain (Schimel et al., 2001; Houghton, 2007). During the past decades, considerable efforts have been made to develop process-based carbon cycle models, as tools to understand terrestrial carbon mechanisms and fluxes at local, regional, continental and global scales (Moorcroft et al., 2006; Huntingford et al., 2011). Models were applied to hindcast historical changes (Cramer et al., 2001; Piao et al. 2009), and to forecast future changes (Friedlingstein et al., 2006; Sitch et al; 2008). Although carbon cycle models have been tested against CO_2 fluxes measured by eddy-covariance technique at sites around the world (Sitch et al., 2003; Krinner et al., 2005; Jung et al., 2007; Stockli et al. 2008; Wang et al. 2012; Keenan et al. 2012), satellite based leaf area index (LAI) retrieval products (Lucht et al., 2002; Piao et al., 2006, 2008), and observed vegetation productivity and carbon storage (Randerson et al., 2009), it is difficult to draw a clear picture of model performance and shortcomings from the current model-benchmarking literature dealing with the global terrestrial carbon cycle. The reasons for this are several: 1) *in situ* high-quality measurements are very sparse, and often cannot be extrapolated readily to larger spatial scales, 2) satellite measurements provide only indirect proxies of carbon variables, 3) atmospheric CO_2 evaluates the combination of a terrestrial carbon model, atmospheric transport model and potentially ocean carbon models, and as such the results thus depend on the choice of the atmospheric transport model and its bias (Stephens et al. 2007), 4) uncertainties associated with measurements are often not reported, which generates type-1 error (a model is estimated to be realistic but the benchmark measurement is not accurate enough to say this) and type-2 error (a model is estimated to be erroneous, whereas the benchmark data is biased), and 5) several recent studies have documented prototype benchmark schemes for the carbon cycle (Randerson et al., 2009, Cadule et al., 2010; Blyth et al., 2011), however, a community-wide set of agreed benchmark tests and performance indicators is currently still under development.

Current coupled-climate-carbon models used in the 4th and 5th Assessment Reports of IPCC generally project a positive feedback between global warming and the reduction of terrestrial carbon sinks in the 21st century (Denman et al., 2007). In some instances, these feedbacks become stronger over time than the CO_2-induced fertilization and hence the land surface has the potential to eventually become an overall source (Cox et al., 2000). Characterizing this feedback has important implications for mitigation policies designed to stabilize greenhouse gas levels (Matthews, 2005). The magnitude of this positive feedback varies markedly among models (Friedlingstein et al., 2006). For the SRES-A2 CO2 emission scenario, by 2100 the modelled climate-carbon cycle feedback is estimated to cause an additional increase in CO_2 content of between 20 ppmv to 200 ppmv, which corresponds to an additional global temperature increase of 0.1˚C–1.5˚C (Friedlingstein et al., 2006). This large uncertainty in carbon-climate feedbacks is associated with the different sensitivities of simulated terrestrial carbon cycle processes to changes in climate and atmospheric CO_2 (Friedlingstein et al., 2006; Huntingford et al., 2009). Other important processes, such as nutrient constraints, may further affect terrestrial carbon climate interactions (Arneth et al. 2010, Zaehle & Dalmonech, 2011).

In this study, a set of ten process-based models is tested for their ability to predict current global carbon fluxes (GPP, NPP & NBP) and their sensitivity to climate variability and rising atmospheric CO_2 concentration. The model ensemble includes: HyLand (Levy et al., 2004), Lund-Potsdam-Jena DGVM (Sitch et al., 2003), ORCHIDEE (Krinner et al., 2005), Sheffield–DGVM (Woodward et al., 1995; Woodward and Lomas, 2004), TRIFFID (Cox, 2001), LPJ-GUESS (Smith et al., 2001), NCAR_CLM4C (Oleson et al., 2010; Lawrence et al., 2011), NCAR_CLM4CN (Oleson et al., 2010; Lawrence et al., 2011), OCN (Zaehle & Friend, 2010), and VEGAS (Zeng et al., 2005). We compare the model output of NBP with the RLS from Friedlingstein et al. (2010) (hereafter FR10). For global climatological GPP we compare model results with those from Jung et al. (2011) (hereafter JU11), which is based on the global interpolation of flux tower observations using a model tree ensemble (MTE) regression approach trained with satellite FAPAR and climate fields. Finally, ecosystem controlled warming experiments (six sites) and Free Air CO_2 Enrichment (FACE) experiments (four

sites) are used to test the models' sensitivity of NPP to individual changes in temperature and CO_2.

2. Methods

2.1 Terrestrial carbon cycle models

The 10 carbon cycle models used in this study are briefly described in the Table S1. All models describe surface fluxes of CO_2, water and the dynamics of water and carbon pools in response to change in climate and atmospheric composition. However, the formulation and number of processes primarily responsible for carbon and water exchange differs among models.

Two simulations, S1 and S2, were performed over the period 1860-2009. In S1, models were forced with rising atmospheric CO_2 concentration, while climate was held constant (recycling climate mean and variability from the early decades of the 20th century, e.g. 1901-1920). In S2, models were forced with reconstructed historical climate fields and rising atmospheric CO_2 concentration. All models used the same forcing files, of which historical climate fields were from CRU-NCEP v4 dataset (http://dods.extra.cea.fr/data/p529viov/cruncep/) and global atmospheric CO_2 concentration were from the combination of ice core records and atmospheric observations (Keeling & Whorf, 2005 and update). Details of the simulation settings are described in Sitch et al. (*submitted)*. It should be noted that land use change was not taken into account in S1 and S2.

2.2 Data-oriented global estimation of GPP

Direct observation of Gross Primary Production (GPP) at the global scale does not exist. Thus, we used a GPP gridded data product from a Multiple Tree Ensemble (MTE) model-data fusion scheme involving eddy covariance flux tower data, climate, and satellite FAPAR fields (Jung et al., 2011 for description of the method), available during 1982-2008, to compare with model output. In the MTE method employed by JU11, a set of regression trees were trained with local GPP estimation from eddy flux NEE measurements with the Lasslop et al. (2010) method used to separate GPP, and 29 candidate predictor climate and biophysical variables, including vegetation types, observed temperature, precipitation and radiation, and satellite

derived fraction of absorbed photosynthetic active radiation (FAPAR). The ensemble of the trained regression trees was driven by global fields of predictor variables to derive gridded GPP estimates (Beer et al., 2010). Uncertainty of the GPP estimated from MTE is relatively small, at about ± 6 Pg C yr^{-1} (Jung et al., 2011). However, this does not consider other sources of uncertainty such as measurement uncertainties of eddy covariance fluxes, of global predictor variables as well as sampling bias driven by unevenly distributed eddy covariance flux sites, with many sites in temperate regions and very few sites in the tropics. As described further below, this dataset should also be used with extreme caution for assessment of interannual variability of GPP.

2.3 The 'residual' land sink (RLS)

The RLS of anthropogenic CO_2 during the period 1980-2009 is taken from the Global Carbon Project carbon budget from Friedlingstein et al. (2010) and Le Quéré et al.(2009). It is estimated as a residual of all other terms that compose the global carbon budget, since no direct global observation of land carbon balance is otherwise available, except for the global forest sink (Pan et al., 2011). The RLS is the sum of fossil fuel and cement emissions and land use change emissions minus the sum of observed atmospheric CO_2 growth rate and modeled ocean sink. The CO_2 emissions from fossil fuel and cement are estimated based on statistics provided by United Nations Energy Statistics (Marland et al., 2005), British Petroleum statistic review of world energy (http://www.bp.com/productlanding.do?categoryId=6929&contentId=7044622), and USGS statistics on cement production (Van Oss, 2006). Emissions from land use change (Houghton, 1999) are based on statistics published by the United Nations Food and Agriculture Organization and a book-keeping model (Houghton, 2010). Atmospheric annual CO_2 growth rate is derived from the NOAA/ESRL global cooperative air-sampling network (Conway et al., 1994). The ocean sink of anthropogenic CO_2 is calculated from the average of four ocean carbon cycle models (Le Quéré et al., 2009). It is important to note that the net land use source estimate in FR10 is 0.3 Pg C yr^{-1} lower over 2000-2009 than the previous LUC emission estimate (Le Quéré et al., 2009). This lower estimate uses the same Houghton et al. model, but takes as input data updated information on forest area change from (FAO, TBRFA

2010) instead of the TBFRA 2005. A lower LUC emission estimate results in a lower RLS mean value.

2.4 Field ecosystem warming experiment

Data from a harmonized field warming experiment dataset compiled from 124 published papers (Lu et al., submitted) was used to evaluate model performance. In order to compare with model outputs, available observations of Net Primary Production (NPP) in experimental sites with warming only treatments and the control experiment were used in our study. The six available sites were located over the temperate and boreal northern hemisphere between 30ºN - 70ºN with mean annual temperature spanning from -7 ºC to 16 ºC and mean annual precipitation spanning from 320 mm to 818 mm (Table S2). The magnitude of experimental warming ranges from 1ºC to 3.5 ºC among different treatments and different sites. These levels of warming are of a magnitude equal or higher than inter-annual variability of temperature, and so complement comparison of simulations S2 and their testing against data, where for the latter an emphasis might be placed on anomalously warm years. It should be noted that total NPP (both aboveground and belowground NPP) were measured in four of the sites, while the other two sites (HARS and Toolik Lake) only measured aboveground NPP.

2.5 Free Air Carbon Dioxide Enrichment (FACE) experiments

Free Air Carbon Dioxide Enrichment (FACE) experiment provided field experimental data on the response of NPP to elevated CO_2. Four FACE experiments in temperate forest stands provided data for our evaluation (Table S3). NPP was calculated as annual carbon increments in all plant parts plus the major inputs to detritus, litterfall, and fine root turnover. We used data from Norby et al. (2005), however data from the ORNL FACE site was corrected and extended to 2008 (Iversen et al., 2008). Data from young stands in the early stage of sapling development with expanding canopies, and some plots with increasing O_3 at the ASPEN FACE were not included in the dataset, as described by Norby et al. (2005). There were in total 21 site-year NPP observations available for our study. Site characteristics and experiment settings in each stand can be found in Table S3, with a more detailed description given in Norby et al. (2005). There are no FACE experiments for tropical ecosystems.

2.6 Analysis

2.6.1 Response of carbon fluxes to climate variations

We estimate empirically the response of GPP, NPP and NBP to climate variability (MAT and annual precipitation) over the last three decades by using a multiple regression approach (Eq. 1):

$$y = \gamma^{int}\, x_T + \delta^{int}\, x_P + \varepsilon \qquad (Eq.\,1)$$

where y is the detrended anomaly of the carbon fluxes GPP, NPP and NBP from the S2 simulations (i.e. simulations considering change in both climate and atmospheric CO_2 concentration, see section 2.1) estimated by each model. Equation (1) is also fitted to the data-oriented model of GPP (JU11 GPP) and to the RLS values from FR10. The variable x_T is the detrended MAT anomaly, and x_P is the detrended annual precipitation anomaly. The fitted regression coefficients γ^{int} and δ^{int} define an *apparent* carbon flux sensitivity to interannual variations in temperature and precipitation, and ε the residual error term. Note that γ^{int} (or δ^{int}) reflect the contributive effect of temperature (or precipitation) variations on carbon fluxes, but not the 'true' sensitivities of these fluxes, given that: (1) temperature and precipitation co-vary over the time, and (2) other climate drivers discarded in Eq.1, such as solar radiation, humidity, and wind speed may also contribute to the variability of detrended carbon fluxes. The regression coefficients are calculated using maximum likelihood estimates (MLE). The uncertainty in γ^{int} and δ^{int} was estimated using the standard error of the corresponding regression coefficients. Data from 1980 to 2009 were used to quantify the response of carbon fluxes to climate variations, except for GPP where instead the period 1982-2008 was considered in order to be consistent with the period covered by the JU11 data-oriented estimate. In order to be consistent with RLS, we first aggregate each grid cell carbon flux into a global mean flux (see SI) and then remove the trend using a least squares linear fitting method.

2.6.2 Response of carbon fluxes to CO_2 trended over the past 30 years

Two approaches were applied to estimate the response of carbon fluxes to CO_2 (β). In the

first approach, β was estimated based on S1 simulations (i.e. the simulations that only consider change in atmospheric CO_2 concentration) using Eq. (2):

$$\beta = \frac{\Delta F}{\Delta CO2} \qquad \text{(Eq. 2)}$$

where, △F is the difference of average carbon fluxes between the last and the first five years of the S1 simulation, while △CO2 is the corresponding change in atmospheric CO_2 concentration. In order to estimate the uncertainty of β, we also calculated the change in carbon fluxes and CO_2 over the study period by randomly selecting a different year over the first and last five year period.

In the second approach, we used a multiple regression approach (Eq. 3) to estimate β for RLS, or for JU11's GPP, and for each model's carbon flux from simulation S2 (both climate and CO_2 change).

$$y = \beta\, CO_2 + a\, Tmp + b\, Prcp + c + \varepsilon \qquad \text{(Eq. 3)}$$

where, y is the carbon flux of each model from S2, or RLS from FR10, and CO_2, Tmp, and Prcp are the atmospheric CO_2 concentration, MAT and annual precipitation respectively. Quantities β, a, b, and c are regression coefficients, while ε is the residual error term. The regression coefficients are calculated using maximum likelihood estimates (MLE). Our Eq. 3 attributes the time series of the y flux to what we consider as the dominant drivers of change i.e. temperature, precipitation, and CO_2. However we do recognize that other land surface changes or meteorological forcing might influence too, and these become implicit in our regression co-efficients. Such effects are for example land use, forest demography, nitrogen deposition, solar radiation, humidity, and wind speed, which influence the trend of RLS time series. Therefore, although we believe rising CO_2 to be strongly influencing the RLS trend the precise values of our regression co-efficients should be treated with caution. Generally, a and b indicate the contributive effect of temperature (resp. precipitation) variations on the carbon fluxes variations (Fig. S1). The period 1980-2009 is used to estimate the carbon fluxes sensitivities to climate and CO_2, except for GPP where the period considered is 1982-2008.

2.6.3 Temperature sensitivities of vegetation productivity derived warming experiment

For warming experiments, the sensitivity of NPP to an (generally stepwise) applied change in temperature, is estimated as the ratio of the relative difference between NPP in warmed minus control plots to the applied warming magnitude. The estimated temperature sensitivity at each experimental site is then compared with the ratio of $\gamma_{NPP}^{\text{int}}$ estimated from model simulations and with the multiple regression method (Eq. 1). This corresponds to the 30-year average NPP (hereafter $R\gamma_{NPP}^{\text{int}}$), and with models being sampled at the grid point containing the experimental site. In addition, we also extract modeled sensitivities in 'climate neighbours' grid points where the mean annual temperature differs by less than 1°C and mean annual precipitation by less than 50 mm from the conditions at each experimental site. Only neighbouring grid points with the same dominant vegetation cover as observed at each experimental site are retained, e.g. for grassland warming sites; all grid points with grassland cover of less than 50% are excluded. Since models do not explicitly represent wetland processes, we grouped wetland with grasslands. Using a similar approach, we estimated the sensitivities of NPP to rising atmospheric CO_2 concentration from the FACE sites and the relative response of NPP to CO_2 ($R\beta_{NPP}$, the ratio of β_{NPP} estimated by Eq. 2 to the 30-year average NPP in each model).

We note that due to this set-up, we cannot make quantitative statements about the nature of the model-data agreement. Both, the step-wise nature of the experiment and the magnitude of the perturbation may induce non-linear effects in the ecosystems that cannot (and should not) be reproduced by ecosystem models simulating the consequences of a gradual and less pronounced perturbation over the last three decades. In particular, because of the saturating effect of CO_2 on leaf level photosynthesis, we expect to see a larger relative effect of CO_2 on photosynthesis when evaluating the increase from 338 to 386 ppm than the response from field experiments elevating CO_2 concentration from about 360 to 550 ppm.

3. Vegetation productivity

3.1 GPP estimation

Global terrestrial GPP averaged across 10 models is 133±15 Pg C yr^{-1}, ranging from

111±4 Pg C yr^{-1} (±s.d. of GPP over the three decades) in SDGVM to 151±4 Pg C yr^{-1} in ORCHIDEE and CLM4C. The higher estimates are consistent with the inferred estimate from ^{18}OCO in the atmosphere (Welp et al., 2011), although this high value is also uncertain and in contrast to earlier studies (Ciais et al., 1995, Beer et al. 2010). The JU11 GPP product derived from eddy-covariance flux towers, generally gives a lower estimate of GPP than the majority of the processed-based models (Fig. 1), particularly in temperate regions (Fig. S2b). At the global scale, the magnitude of GPP (113±3 Pg C yr^{-1}) in LPJ-GUESS is close to JU11 (118±1 Pg C yr^{-1}). However, this result should be viewed with caution, since a similar global magnitude can mask compensation of biases between tropical and non-tropical regions. As shown in Fig. S2 and S3, the LPJ-GUESS simulation has a low bias of GPP in tropical regions compared to JU11 (68% of JU11), compensated by a high bias in non-tropical regions.

At the global scale, the correlation of interannual GPP variations among the different models is much higher than that with JU11 as shown by Fig. 2a. JU11 GPP is estimated from satellite and eddy covariance flux tower measurements, and flux tower sites are mainly distributed in northern temperate regions (mainly forest). Hence a larger sampling uncertainty is associated with JU11 for GPP outside this northern region. This is of importance as tropical ecosystems are largely driving the interannual variability of the carbon cycle (Denman et al., 2007). Interestingly, the lowest correlation between GPP from models and JU11 is found in tropical regions (Fig. S4c) perhaps due to fewer eddy-covariance flux sites available to create the interpolated global product. Furthermore, the standard deviation of GPP is found to be substantially higher in the 10 process models than in JU11 (compare error bars in Fig. 1a), and particularly over tropical regions (Fig. S2c). This leads us to make the hypothesis that the GPP interannual variability is under-sampled in JU11 and hence systematically lower than the interannual variability simulated by the DGVMs. This hypothesis is further discussed in the next section.

3.2 Response of GPP to temperature variations ($\gamma_{GPP}^{\text{int}}$)

At the global scale, the models suggest that interannual variation in global GPP is not significantly correlated with temperature (all variables detrended), as can be seen from the large differences in the magnitude and even in the sign of the γ_{GPP}^{int} (Fig. 3a) due to the different sensitivity values over different regions (Fig. S6). In the tropical regions, all models have a negative apparent sensitivity γ_{GPP}^{int} (-2.2±1.2 Pg C yr^{-1} $^{o}C^{-1}$ or -2.9±1.4 % $^{o}C^{-1}$; significant for 7 out of 10 models), while JU11 has a positive γ_{GPP}^{int} (0.4±0.7 Pg C yr^{-1} $^{o}C^{-1}$ or 0.6±1.0 % $^{o}C^{-1}$, P>0.05) (Fig. S6c). JU11's GPP response to temperature variability over tropical regions, however, may be considered as more uncertain than models, since satellite FAPAR used by JU11 for spatial-temporal interpolation of GPP distribution between flux tower locations is often contaminated by cloudiness (Myneni et al., 1997). Furthermore, JU11 trained their MTE using *spatial gradients* among different sites (there are few long series) and then used the derived relationship to extrapolate to *temporal* interannual gradients. This assumes that spatial and interannual sensitivity of GPP to climate are the same, which may be not correct. Measurements of tree growth in tropical forests have shown negative correlation with temperature (Clark et al., 2003; Clark et al., 2008). This result is also supported by short-term leaf level measurements in tropical forests which indicate a decrease in net carbon assimilation at higher temperature (Tribuzy, 2005; Doughty and Goulden, 2008). This negative response of vegetation productivity to MAT variability may arise from the fact that tropical forests already operate near to a high temperature optimum threshold above which vegetation photosynthesis declines sharply (Corlett et al., 2011).

In boreal regions, vegetation growth is limited by temperature which controls the length of the growing-season, implying that rising MAT causes an extension of the growing season, and induces an increase in GPP (Piao et al. 2007; Richardson et al., 2010). It has been suggested that rising temperature is enhancing vegetation growth in boreal regions (Lucht et al., 2002; Piao et al., 2006; Piao et al., 2009; Wang et al., 2011) except in regions affected by summer drought, during the analysis period, such as parts of Alaska (Beck et al., 2011). All the models show significant positive relationship (P<0.05) between boreal GPP and MAT with

an average γ_{GPP}^{int} of 0.8±0.3 Pg C yr^{-1} $^{o}C^{-1}$ (or 4.5±1.5 % $^{o}C^{-1}$), which is close to the γ_{GPP}^{int} derived from the GPP of JU11 (0.9±0.3 Pg C yr^{-1} $^{o}C^{-1}$ or 4.7±1.5% $^{o}C^{-1}$) (Fig. S6a).

In temperate regions, the response of GPP to MAT depends partly on the balance between the positive effect of warming through extending the growing season in spring and possibly in autumn (although recent work suggest that the photoperiod may limit GPP, Bauerle et al., 2012), reaching more optimal growing temperature, and the negative effect of warming through enhanced soil moisture stress in summer. At the regional scale, most models (except CLM4CN and HYLAND) and JU11 data-product show a non-significant interannual correlation between MAT and GPP (Fig. S6b).

3.3 Comparison with the field warming experiments

Fig. 4 shows the spatial distribution of the $R\gamma_{NPP}^{int}$ (the ratio of γ_{NPP}^{int} to the 30-years average NPP of each model) averaged across the 10 models. Similar to the regional scale analyses of γ_{GPP}^{int} above, we checked for a positive (resp. negative) interannual correlation between MAT and NPP in boreal (resp. tropical) regions. We then compared the simulated $R\gamma_{NPP}^{int}$ against the relative sensitivity derived from field warming experiments, which are only distributed over the northern hemisphere. Field warming experiments show that rising temperature generally increases NPP (after 4 years of warming on average) across most sites, except at the Haibei Alpine Research Station (in the Tibet Plateau) where rising temperature significantly decreased aboveground NPP by -8% $^{o}C^{-1}$ (Fig. 4). The sign of this sensitivity in Haibei Alpine Research Station is correctly captured by six of ten models (Fig. 4). One can also see in Fig. 4 that models tend to predict smaller $R\gamma_{NPP}^{int}$ values than observed at the warming experiment temperate sites, particularly at Jasper Ridge Global Change Experiment (JRGCE), Kessler's Farm Field Laboratory (KFFL), Toivola and Alborn (Minnesota 2), and Duolun. One can assume that this may be because in the grid points containing these sites, annual precipitation used in model forcing is less than actual precipitation at field sites (by 15% at Jasper Ridge Global Change Experiment, 8% at Kessler's Farm Field Laboratory, 46%

at Toivola and Alborn, and 17% at Duolun). The results of two field warming experiment sites in Minnesota, USA (47°N, 92°W) have shown that the wetter site (annual precipitation of 762 mm) has a much higher NPP sensitivity to warming (12 - 22 % $^{o}C^{-1}$ yr^{-1}) than the drier site (annual precipitation of 497 mm, -3 - 6 % $^{o}C^{-1}$ yr^{-1}) (Fig. 4), implying that average climatic conditions (in particular through soil moisture availability) regulate the response of NPP to temperature. To mini minimize the effect of biases in the climate drivers, we also extract modeled sensitivities in 'climate neighbours' grid points where the mean annual temperature differs by less than 1^{o}C and mean annual precipitation by less than 50 mm from the conditions at each experimental site. As shown in Fig. 4, however, the model estimated at JRGCE, KFFL, Minnesota 2, and Duolun, is still systematically lower than observation, implying that the different forcing may be not the primary reason the mismatch between models and observations. A recent study comparing model simulations driven by site-level climate forcing and by gridded climate forcing suggested that model structure, rather than climate forcing, remained the main limitation for improving model-site data comparison (Rackza et al., submitted).

In addition, it should be noted that the methods we used to quantify the response of NPP to temperature change in models (interannual variability) and in field warming experiments (multi-years treatments have a higher amplitude of stepwise warming than the inter-annual range of natural variability, and no covariate precipitation change) are different, which may cause inconsistencies in evaluating models. Even at the same site, the magnitude of the temperature sensitivity of NPP depends upon the magnitude of warming. For example, field warming experiments at the drier site in Minnesota, USA (47°N, 92°W), show that temperature sensitivity of NPP for a step 2 ^{o}C warming (1 - 6% yr^{-1}) is larger than that for a step 3 ^{o}C warming (-3 - 2% yr^{-1}). Furthermore, $R\gamma_{NPP}^{\mathrm{int}}$ of processed-based models does not consider local heterogeneity of environmental conditions and land cover, and local biogeophysical feedbacks (e.g., Long et al. 2006). This spatial scale mismatch adds uncertainty to model evaluation using warming experiment sites. For instance, the temperature sensitivity of NPP derived from the warming experiment at the two Minnesota

sites (47°N, 92°W) that are located in the same grid point of models, varies from -3% $^{o}C^{-1}$ to 22% $^{o}C^{-1}$, which is a larger range than that predicted by the models over the corresponding grid point (from -2.7% $^{o}C^{-1}$ to 6.1% $^{o}C^{-1}$). In addition, the models may not fully represent ecosystem-level mechanisms underlying NPP responses to warming in experiments, such as warming-induced changes in nutrient availability, soil moisture, phenology, and species composition (Luo, 2007). Overall, the inconsistency of the response of NPP to temperature change between models and field warming experiments should be addressed by further studies, for instance running the same models with site observed forcing data and vegetation, soil parameters.

3.4 Response of GPP to precipitation variations ($\delta_{GPP}^{\text{int}}$)

Over the past few decades, many regions have experienced drought, which has a negative effect on vegetation productivity (Zhao et al., 2010 for the globe; Angert et al., 2005 and Zeng et al., 2005 for the Northern Hemisphere; Ciais et al., 2005 for Europe; Zhang et al., 2010 for North America; Potter et al., 2011 for Amazonia, McGrath et al., 2012 for Australia, Wang et al., 2010 for China). Droughts that occurred from 1998 to 2002 in the northern hemisphere mid-latitudes, for example, led to an estimated reduction of vegetation NPP by 5% compared to the average of the previous two decades (Zeng et al., 2005). Although individual drought events cannot be attributed to anthropogenically-induced climate change, there is a concern that a general situation of more extreme weather events is emerging, including the potential for alteration to the global hydrological cycle. Over the northern hemisphere, all models have a positive $\delta_{GPP}^{\text{int}}$. However the interannual correlation between GPP and precipitation was found not significant for JU11, HYLAND, LPJ-GUESS, and VEGAS in boreal regions (Fig. S7a), and JU11, HYLAND in northern temperate regions (Fig. S7b).

There has been much discussion in the literature about the impact of drought on vegetation growth and mortality in tropical regions (Nepstad et al., 2004; Da Costa et al., 2010; Phillips et al., 2009 and 2010). A rainfall exclusion experiment in an east-central

Amazonian rainforest at Tapajos showed that a 50% reduction in precipitation led to a 25% reduction in vegetation NPP over the first two years of the experiment (Nepstad et al., 2002). It has been suggested that spatial GPP variability in 30% of tropical forest and in 55% of tropical savannahs and grasslands is primary correlated with the precipitation (Beer et al., 2010). Indeed, at the continental scale, all models show a positive correlation of GPP with annual precipitation over tropical regions (not significant in JU11 and HYLAND), but the magnitude of $\delta_{GPP}^{\text{int}}$ differs among models with TRIFFID and LPJ having the largest $\delta_{GPP}^{\text{int}}$ (about 2.2±0.4 Pg C yr^{-1} per 100 mm or 2.8±0.5 % per 100 mm for TRIFFID, and 1.8±0.4 Pg C yr^{-1} per 100 mm or 2.7±0.5 % per 100 mm for LPJ) (Fig. S7c). The average of tropical $\delta_{GPP}^{\text{int}}$ across the 10 models is 1.4±0.5 Pg C yr^{-1} per 100 mm (or 1.8±0.7% per 100 mm), which is three times larger than $\delta_{GPP}^{\text{int}}$ of the JU11 data-oriented GPP (0.5±0.3 Pg C yr^{-1} per 100 mm or 0.6±0.4 % per 100 mm).

Overall, at the global scale, $\delta_{GPP}^{\text{int}}$ averaged across the 10 models is 4.1±2.0 Pg C yr^{-1} per 100 mm (or 3.1±1.5% per 100 mm) (Fig. 3b). Among the 10 models, 8 exhibit significant correlations between global GPP and annual precipitation (all variables detrended). Considering that global GPP was not correlated with MAT in any of the models (see section 3.2.1), we conclude that interannual variation of GPP is more closely controlled by precipitation rather than by temperature (Piao et a., 2009; Jung et al., 2011). The TRIFFID model has the highest $\delta_{GPP}^{\text{int}}$ (7.6±1.5 Pg C yr^{-1} per 100 mm or 5.5±1.1% per 100 mm) as seen in Fig. 3b. Differences in simulated land cover between models, in addition to structural sensitivities (i.e., sensitivity of stomata to soil moisture) may also explain the variability among models, particularly in arid and temperate regions (Poulter et al. 2011).

3.5 Response of vegetation productivity to CO_2

According to the results of simulation S1 driven by atmospheric CO_2 only, model results consistently indicate that rising atmospheric CO_2 concentration increased NPP by 3-10% with an average of 7% over the past three decades (for a 48 ppm CO_2 increase) (or 0.05-0.2 %

ppm^{-1} with the average of 0.16 % ppm^{-1}). This relative response of NPP to CO_2 ($R\beta_{NPP}$) is slightly larger than the sensitivity derived from FACE elevated CO_2 experiments, which might be expected because of the saturating effect of CO_2 on photosynthesis. Norby et al. (2005) analyzed the response of NPP to elevated CO_2 in four FACE experiments in temperate forest stands and concluded that the enhancement of NPP due to elevated CO_2 (about 180 ppmv) was of about 23% (or 0.13% ppm^{-1}). When comparing the results from the four FACE experiments with model simulations at the corresponding sites and climatic condition, however, we found that the models underestimated CO_2 fertilization effect on NPP at the ASPEN FACE site, but overestimated it at the Duke and ORNL FACE sites (Fig. 6). The study of Hickler et al. (2008) suggested that these currently available FACE results are not applicable to vegetation globally since there may be large spatial heterogeneity of the positive effect of CO_2 on vegetation productivity across the global land surface. Hence we do not present the FACE values in global plot Fig 5a. As shown in Fig. 6, the modeled response of NPP to CO_2 is generally larger in dryer regions. Among the four FACE experimental sites, a largest CO_2 fertilization effect of NPP was also found in the driest (ASPEN FACE) site (Fig. 6 and Table S3). This NPP enhancement could be due to the additional saving of soil moisture induced by elevated CO_2 on stomatal closure (i.e. increased water use efficiency of plants in water limited regions).

It has been suggested that the CO_2 fertilization effect on vegetation productivity may be overestimated by not considering N limitations (Hungate et al., 2003; Bonan and Levis, 2010; Zaehle et al., 2010). As in Bonan and Levis 2010, we find that for CLM4, β_{GPP} in the CLM4CN that considers C-N interaction and N limitations is lower than that estimated in the CLM4C without C-N interaction (Fig 5a). In boreal regions, β_{GPP} of CLM4CN (2.2±1.4Pg C yr^{-1} per 100 ppm or 12±8% per 100 ppm) is only about half of CLM4C estimated β_{GPP} (4.4±1.5Pg C yr^{-1} per 100 ppm 21±7% per 100 ppm). As noted previously (Zaehle & Dalmonech 2011), there is a difference in the extend of N limitation on global carbon cycling between CLM4C-N and OCN, although both of them have N limitations on GPP. OCN

predicts a relatively high β_{GPP}, particularly in tropical regions (12.7±1.6 Pg C yr^{-1} per 100ppm or 18±2% per 100ppm), which is two times larger than that estimated by CLM4CN (6.6±1.2 Pg C yr^{-1} per 100ppm or 7±1% per 100ppm) (Fig. S9c).

According to equation (3), the GPP data-driven product of JU11 shows weak sensitivity to CO_2 at the global scale (Fig. 5a), although satellite data used to drive the empirical model of Jung et al. (2011) includes a greening trend whose spatial pattern can be partly accounted for by rising CO_2 (Piao et al., 2006). Furthermore, the model results show that β_{GPP} derived from simulations S2 (i.e. consider both climate change and rising atmospheric CO_2 concentration and equation (3)) are generally larger than β_{GPP} from simulation S1 that only consider rising atmospheric CO_2 concentration (Fig. 5a). This is particularly true in the tropical regions (Fig. S9c). This may be partly because the mean climate in the early decades of the 20th century for S1 simulation is wetter than that in end decades of the 20th century for S2 simulation in the tropical regions (IPCC, 2007), or indicate that the linear regression approach does not replicate the intricate non-linear complexity of the global carbon cycle.

4 Net Biome Productivity

4.1 NBP estimation

Global NBP is not significantly correlated with the global GPP across 10 models (R=0.48, P=0.16) (Fig. 1), suggesting that models predicting larger GPP does not necessarily translate into larger NBP. The ensembles model average NBP (all without land use change) during the period 1980-2009 is 2.0±0.8 Pg C yr^{-1}, which is very close to the RLS of 2.1±1.2 Pg C yr^{-1}. However, there are large differences among different models, with NBP ranging from 0.24±1.03 Pg C yr^{-1} (VEGAS) to 3.04±0.98 Pg C yr^{-1} (HYLAND) (Fig. 1). The smaller NBP of VEGAS is related to the net tropical carbon source produced by this model (-0.12±0.9 Pg C yr^{-1}). In contrast, the other 9 models (in absence of land-use) produce a net sink of 1.13±0.44 Pg C yr^{-1} on average (Fig. S2c), explaining 54% of global RLS.

In addition, for analysis of the interannual variability in modeled global NBP from 1980

to 2009, all models show generally good agreement with the observed variability of the RLS ($P<0.05$) (Fig. 2b). Interestingly, for NBP variability, CLM4CN has a lower correlation with RLS than CLM4C (Fig. 2b), implying that in this particular model, incorporation of the nitrogen cycle does not improve the performance for interannual variability, which may reflect model structural problems in describing processes controlling C-N interactions (Bonan and Levis, 2010). Note, however, that a strong dampening of the interannual variability in the carbon cycle is not a general feature of nitrogen dynamics (Zaehle et al. 2010). In addition, at the regional scale, the correlation of interannual NBP among different models is higher in the tropical regions than that in non-tropical regions (Fig. S5).

4.2 Response of NBP to temperature variations ($\gamma_{NBP}^{\text{int}}$)

Direct observational evidence for a positive feedback of the terrestrial carbon cycle to climate warming is limited (Scheffer et al., 2006; Cox and Jones, 2008; Frank et al., 2010). Applying the regression of Equation (1) to RLS timeseries defines an 'observed' contributive effect of temperature variations on the RLS variations ($\gamma_{RLS}^{\text{int}}$) of -3.9±1.1 Pg C yr-1 $^{o}C^{-1}$ (Fig. 3a), which is larger than, but within the uncertainty range of $\gamma_{NBP}^{\text{int}}$ in the 10 models (-3.0±1.5 Pg C yr^{-1} $^{o}C^{-1}$). Except for HYLAND and SDGVM, 8 out of 10 models show significant negative correlation between NBP and MAT, but $\gamma_{NBP}^{\text{int}}$ varies among models from -1.0±0.6 Pg C yr^{-1} $^{o}C^{-1}$ in HYLAND to -5.1±0.9 Pg C yr^{-1} $^{o}C^{-1}$ in LPJ-GUESS. Such difference in across 10 models mainly depends on model differences in the response of GPP to temperature ($R=0.63$, $P=0.05$), rather than response of respiration to temperature ($R=0.44$, $P>0.05$). Furthermore, the contribution of fire to the is also limited (Fig. S8a). The value of $\gamma_{NBP}^{\text{int}}$ in CLM4CN (-2.1±0.5 Pg C yr^{-1} $^{o}C^{-1}$) is only half of that in CLM4C (-4.3±0.8 Pg C yr^{-1} $^{o}C^{-1}$), which may be partly because during warmer years, increased soil nitrogen mineralization and availability may promote vegetation growth (Melillo et al., 2002). However, $\gamma_{NBP}^{\text{int}}$ from CLM4C is closer to the observed $\gamma_{RLS}^{\text{int}}$ that for CLM4CN.

The negative value of global γ_{NBP}^{int} is mainly due to negative NBP anomalies (abnormal CO_2 source to the atmosphere) occurring during warm years over tropical regions (Fig. S6c). All models show statistically significant interannual correlation of NBP with MAT in the tropical regions (R <0.05), and an average γ_{NBP}^{int} of -3.0 ±1.2 Pg C yr^{-1} $^oC^{-1}$. Compared with tropical regions, other regions have a relatively smaller γ_{NBP}^{int} (Fig. S6). In the boreal zone, there are large differences in the magnitude and even in the sign of γ_{NBP}^{int} among models. For example, LPJ, LPJ-GUESS, and TRIFFID have a γ_{NBP}^{int} of -0.37 ±0.13 Pg C yr^{-1} $^oC^{-1}$, -0.53 ±0.19 Pg C yr^{-1} $^oC^{-1}$, and -0.29 ±0.1 Pg C yr^{-1} $^oC^{-1}$, respectively, but VEGAS has a positive γ_{NBP}^{int} of 0.23 ±0.08 Pg C yr^{-1} $^oC^{-1}$ (Fig. S6a) due to its highest γ_{GPP}^{int} (Fig. S6a). Such model divergence on over boreal zone and the consistency in the sign of over tropical zone can explain why models agree more on the interannual variation of tropical NBP than on the interannual variations of boreal NBP (Fig. S5a and c). In the northern temperate regions, all models (except CLM4CN) show negative γ_{NBP}^{int} with average of -0.44 ±0.45 Pg C yr^{-1} $^oC^{-1}$ (Fig. S6b).

4.3 Response of NBP to precipitation variations (δ_{NBP}^{int})

The RLS is not significantly correlated with the precipitation (after statistically removing the contributive effect of temperature using partial correlation) at the global scale, but in contrast, 8 of 10 models still have a significant positive correlation between NBP and precipitation (all variables detrended) (Fig. 3b). Furthermore, 9 models (except LPJ-GUESS) estimate a higher δ_{NBP}^{int} (average of 2.3±1.6 Pg C yr^{-1} per 100 mm of interannual precipitation change) compared to the observed RLS (0.8±1.1 Pg C yr^{-1} per 100 mm of interannual precipitation change) (Fig. 3b). These results indicate that current state-of-the-art carbon cycle models are likely to be too sensitive to precipitation variability. TRIFFID has the highest δ_{NBP}^{int} sensitivity (6.0±0.9 Pg C yr^{-1} per 100 mm) due to highest. At the global scale, is significantly increased with the increase in by the slope of 0.61 across 10 models (R=0.81,

P<0.01). In addition, the model estimated response fire emission to precipitation is much smaller than the inter-model differences in (Fig. S8).

It has been suggested that decreased CO_2 sinks in the next century over tropical regions, in response to soil drying, was one of the principal mechanisms explaining the positive carbon cycle-climate feedback diagnosed from the C4MIP coupled models (Friedlingstein et al., 2006; Sitch et al., 2008). In the tropics indeed, all models (nine of ten models significant) consistently produce a positive interannual covariance between precipitation and NBP. TRIFFID has the highest tropical $\delta_{NBP}^{\text{int}}$ (1.5±0.2 Pg C yr^{-1} per 100 mm), while ORCHIDEE shows the smallest tropical $\delta_{NBP}^{\text{int}}$ (0.3±0.3 Pg C yr^{-1} per 100 mm). In the extra-tropical regions however, several models predict a negative response of NBP to wetter years, but the NBP-precipitation relationship is generally not significant (HYLAND, CLM4CN, and SDGVM only exhibit a significant relationship in the boreal region, and TFIFFID, LPJ, OCN in the northern temperate regions as shown by Fig. S7). In both boreal and temperate regions, the highest $\delta_{NBP}^{\text{int}}$ was also simulated by the TRIFFID model due to its highest $\delta_{GPP}^{\text{int}}$ (Fig. S7a and b).

4.4 Response of NBP to rising atmospheric CO_2 concentration (β_{NBP})

From the average of the 10 models, we estimated β_{NBP} using simulation S1 to be 2.39 ±1.52 Pg C yr^{-1} per 100 ppm at the global scale. CLM4CN shows the smallest β_{NBP} of 0.54 ±2.79 Pg C yr^{-1} per 100 ppm, which is only 23% of β_{NBP} in CLM4C. This supports results from previous studies that the nutrient limitation of vegetation productivity and carbon sequestration could decrease the land carbon sensitivity to atmosphere CO_2 concentration (Sokolov et al., 2008; Thornton et al., 2009; Zaehle et al., 2010). ORCHIDEE has the largest β_{NBP} of 5.86±2.02 Pg C yr^{-1} per 100 ppm (Fig. 5b), probably due to its highest β_{GPP} compared to other models (Fig. 5a). Indeed, there is a significant correlation between β_{NBP}

and β_{GPP} across 10 models (P<0.05), suggesting that models have different β_{NBP} partly because of the different CO_2 fertilization effect on the vegetation growth (Ciais et al., 2005). Among the 10 models, CLM4CN simulates the lowest carbon sequestration efficiency under rising atmospheric CO_2 concentration (4%), defined as the ratio of β_{NBP} to β_{GPP}, while ORCHIDEE has the highest carbon sequestration efficiency under rising atmospheric CO_2 concentration (20%). The ratio of β_{NBP} to β_{GPP} for the ensemble model average is about 12 ±4%.

Similar to β_{GPP} (Fig. 5a), β_{NBP} derived from simulation S2 and equation (3) is generally larger than β_{NBP} from simulation S1 (Fig. 5b), particularly in tropical regions (Fig. S10c). As shown in Fig. 5b, CLM4CN, OCN, SDGVM, and VEGAS estimated global β_{NBP} from the simulation S2 with equation (3) is smaller than the diagnosed sensitivity of RLS to atmospheric CO_2 (β_{RLS}, 8.12±2.38 Pg C yr^{-1} per 100 ppm) based on equation (3). However, it should be noted that since other factors such as ecosystem management and nitrogen deposition could also explain the trend of RLS over the last three decades (Zaehle et al., 2006; Ciais et al., 2008; Bellassen et al., 2010; Magnani et al., 2007, Zaehle & Dalmonech 2011), the sensitivity of RLS to CO_2 from the equation (3) may be overestimated.

5. From model testing to directions for future research

To overcome the inevitable spread of curves resulting from a comparison of complex models with poorly constrained processes, we compared in this study the *contributive response* of models to climate variability, with available 'observations' (in fact other data-driven models). The main contributive responses to interannual climate drivers are γ – the response to temperature anomalies in units of PgC yr^{-1} $°C^{-1}$, δ – the response to rainfall anomalies in units of PgC yr^{-1} 100 mm^{-1}, and β – the response to CO_2 trend, in units of PgC yr^{-1} 100 ppm^{-1}. Four key datasets are used to estimate these contributive responses, a data-oriented gridded GPP field (JU11), imposed warming experiments, imposed raised

atmospheric CO_2 experiments (FACE) and the global residual land sink modeled to close the anthropogenic CO_2 budget (RLS). These four datasets provide information on different contributive responses, JU11 constrains γ, δ and β of GPP, experimental warming site data constrain γ of NPP, the (scarce) FACE site data constrain β of NPP, and the RLS over 30 years constrains γ, δ and β of NBP. We report the following new findings.

1. The 10 carbon cycle models give a higher mean GPP and a higher year to year GPP variability than JU11, particularly in tropical regions. In tropical regions, the GPP interannual variance in JU11 may however be considered as too uncertain to falsify the process models. JU11 trained their MTE using *spatial gradients* among different sites (there are few long series) and extrapolated *temporal* gradients, confounding spatial and interannual sensitivity of GPP to climate. To overcome this limitations of comparing the uncertain process-models with another uncertain data-driven model, we recommend future work to models at site scale at which the measurements are made (in particular the long term FLUXNET sites) to investigate their response to climate drivers for different time scales, and different ecosystems (Schwalm et al. 2010). This will also require better protocols with site-history to account for site specific disequilibrium of biomass and soil carbon pools (Carvaillhais et al. 2007, 2008).

2. The process models generally capture the interannual variation of the data-driven residual land carbon sink (RLS) estimation over the last three decades. But the models's contributive response to precipitation is too high, particularly in tropical forests and savannas (Wang et al., 2012). It is not clear, however, if this too high contributive response of NBP to rainfall is induced by a bias of GPP or ecosystem respiration to soil moisture, or to an inaccurate representation of soil moisture by models. We recommend future work to compare the contributive response of net and gross CO_2 fluxes between models with independent large-scale flux estimations, such as from data-driven upscaling of fluxes and top down inversions.

3. In response to interannual variation in temperature, all the models are found to simulate a stronger negative response of NBP than GPP, implying that respiration responds positively to temperature. To investigate this effect, we evaluated for the first time the global process models against site-data from a collection of ecosystem warming experiments. We find that models tend to under-predict the response of NPP to temperature change at the

temperate sites. However it is difficult to tell from the warming experiments for NPP, which have significant between-site variation, whether this results predominantly from plant or soil respiration, or possibly both, where the balance varies strongly depending on geographical variation. The different approaches to derive the NPP response to temperature between global models forced offline by gridded climate data, and local field warming experiments that are coupled to the atmosphere, bias as well as the fact that process models do not consider sub-grid scale heterogeneity in environmental conditions and vegetation distribution. We recommend to design a global benchmarking of carbon cycle models against ecosystem warming and drought experiments, and to compile a database of experiments results and forcing data that would be open-access.

4. Despite the fact that carbon cycle models are often suspected to overestimate CO_2 fertilization as a driver of net land uptake, we found that the ensemble mean global NPP enhancement is comparable with FACE experiments observation. The CLM4CN model that have nitrogen limitations do show a sensitivity of NPP to CO_2 that is 50% lower than the same models versions (CLM4C) but without nitrogen. The strength of the CO_2 fertilization on the NBP is poorly quantified. The magnitude of NBP response to CO_2 is not merely dependent on the NPP response. NPP increases could create higher litterfall enhancing soil carbon stores also available to respire. We recommend all carbon cycle models to include nutrients, and pursue the evaluation of C-N interactions using both global and local observations (e.g., Zaehle et al. 2010).

Overall, reducing these uncertainties of climate sensitivities of carbon fluxes is essential to more accurately predict future dynamics of the global carbon cycle and its feedbacks to climate system, and thus it is a priority for the carbon cycle modeling community. We recommend carbon cycle models to be run both "free running" with their default parameters values used in global simulations, and "adjusted" with parameters calibrated or optimized against site observations (e.g, warming, precipitation, and elevated CO_2 experiments, fluxnet data) so that the" portability" of improvements gained from small scale can be assessed at larger, regional or global scale.

Acknowledgements

This study was supported by the Global Carbon Project [www.globalcarbonproject.org], the National Natural Science Foundation of China (grant 41125004), National Basic Research Program of China (Grant No. 2013CB956303 and 2010CB950601), Foundation for Sino-EU research cooperation of Ministry of Science and Technology of China (1003), Chinese Ministry of Environmental Protection Grant (201209031), and CARBONES EU FP7 foundation (242316).

References

Angert A, Biraud S, Bonfils C *et al.* (2005) Drier summers cancel out the CO2 uptake enhancement induced by warmer springs. *Proceedings of the National Academy of Sciences of the United States of America,* **102**, 10823-10827.

Bauerle WL, Oren R, Way DA et al. (2012) Photoperiodic regulation of the seasonal pattern of photosynthetic capacity and the implications for carbon cycling. *Proceedings of the National Academy of Sciences of the United States of America,* www.pnas.org/cgi/doi/10.1073/pnas.1119131109

Beck PS, Juday GP, Alix C *et al.* (2011) Changes in forest productivity across Alaska consistent with biome shift. *Ecology Letters,* **14**, 373-379.

Beer C, Reichstein M, Tomelleri E *et al.* (2010) Terrestrial Gross Carbon Dioxide Uptake: Global Distribution and Covariation with Climate. *Science,* **329**, 834-838.

Bellassen V, Le Maire G, Dhote JF, Ciais P, Viovy N (2010) Modelling forest management within a global vegetation model Part 1: Model structure and general behaviour. *Ecological Modelling,* **221**, 2458-2474.

Blyth E, Clark DB, Ellis R *et al.* (2011) A comprehensive set of benchmark tests for a land surface model of simultaneous fluxes of water and carbon at both the global and seasonal scale. *Geoscientific Model Devvelpment,* **4**, 255-269.

Bonan GB, Levis S (2010) Quantifying carbon-nitrogen feedbacks in the Community Land Model (CLM4). *Geophysical Research Letters,* **37**, L07401, doi:10.1029/2010gl042430.

Cadule P, Friedlingstein P, Bopp L *et al.* (2010) Benchmarking coupled climate-carbon models against long-term atmospheric CO2 measurements. *Global Biogeochemical Cycles,* **24**, GB2016, doi: 10.1029/2009gb003556.

Ciais P, Tans PP, Trolier M, White JWC, Francey RJ (1995) A Large Northern Hemisphere Terrestrial CO2 Sink Indicated by the 13C/12C Ratio of Atmospheric CO2. *Science,* **269**, 1098-1102.

Ciais P, Reichstein M, Viovy N *et al.* (2005) Europe-wide reduction in primary productivity caused by the heat and drought in 2003. *Nature,* **437**, 529-533.

Ciais P, Schelhaas MJ, Zaehle S *et al.* (2008) Carbon accumulation in European forests. *Nature Geoscience,* **1**, 425-429.

Clark DA, Piper SC, Keeling CD, Clark DB (2003) Tropical rain forest tree growth and atmospheric carbon dynamics linked to interannual temperature variation during 1984–2000. *Proceedings of the National Academy of Sciences,* **100**, 5852-5857.

Clark DB, Olivas PC, Oberbauer SF, Clark DA, Ryan MG (2008) First direct landscape-scale measurement of tropical rain forest Leaf Area Index, a key driver of global primary productivity. *Ecology Letters,* **11**, 163-172.

Conway TJ, Tans PP, Waterman LS, Thoning KW, Kitzis DR, Masarie KA, Zhang N (1994) Evidence for interannual variability of the carbon cycle from the National Oceanic and Atmospheric Administration/Climate Monitoring and Diagnostics Laboratory Global Air Sampling Network. *Journal Of Geophysical Research,* **99**, 22831-22855.

Corlett RT (2011) Impacts of warming on tropical lowland rainforests. *Trends in Ecology & Evolution,* **26**, 606-613.

Cox PM, Betts RA, Jones CD, Spall SA, Totterdell IJ (2000) Acceleration of global warming due to carbon-cycle feedbacks in a coupled climate model. *Nature,* **408**, 750-750.

Cox PM (2001) Description of the TRIFFID dynamic global vegetation model. *Technical Note 24 HadleyCentre, Met Office*.

Cox P, Jones C (2008) Illuminating the Modern Dance of Climate and CO2. *Science,* **321**, 1642-1644.

Da Costa ACL, Galbraith D, Almeida S *et al.* (2010) Effect of 7 yr of experimental drought on vegetation dynamics and biomass storage of an eastern Amazonian rainforest. *New Phytologist,* **187**, 579-591.

Denman K, Brasseur G, Chidthaisong A *et al.* (2007) "Couplings Between Changes in the Climate System and Biogeochemistry" in *Climate Change 2007: The*

Physical Science Basis, Contribution of Working Group I to the Fourth Assessment Report of the Intergovernmental Panel on Climate Change, Cambridge University Press, Cambridge, United Kingdom and United States.

Dufresne JL, Fairhead L, Le Treut H *et al.* (2002) On the magnitude of positive feedback between future climate change and the carbon cycle. *Geophysical Research Letters,* **29**, 1405, doi: 10.1029/2001gl013777.

Frank DC, Esper J, Raible CC, Buntgen U, Trouet V, Stocker B, Joos F (2010) Ensemble reconstruction constraints on the global carbon cycle sensitivity to climate. *Nature,* **463**, 527-530.

Friedlingstein P, Cox P, Betts R *et al.* (2006) Climate-carbon cycle feedback analysis: Results from the (CMIP)-M-4 model intercomparison. *Journal of Climate,* **19**, 3337-3353.

Friedlingstein P, Houghton RA, Marland G *et al.* (2010) Update on CO2 emissions. *Nature Geoscience,* **3**, 811-812.

Hickler T, Smith B, Prentice IC, Mj fors K, Miller P, Arneth A, Sykes MT (2008) CO2 fertilization in temperate FACE experiments not representative of boreal and tropical forests. *Global Change Biology,* **14**, 1531-1542.

Houghton RA (1999) The annual net flux of carbon to the atmosphere from changes in land use 1850–1990. *Tellus Series B-chemical And Physical Meteorology,* **51**, 298-313.

Houghton RA (2007) Balancing the global carbon budget. *Annual Review Of Earth And Planetary Sciences,* **35**, 313-347.

Houghton RA (2010) How well do we know the flux of CO2 from land-use change? *Tellus Series B-Chemical And Physical Meteorology,* **62**, 337-351.

Hungate BA, Dukes JS, Shaw MR, Luo YQ, Field CB (2003) Nitrogen and climate change. *Science,* **302**, 1512-1513.

Huntingford C, Lowe JA, Booth BBB, Jones CD, Harris GR, Gohar LK, Meir P (2009) Contributions of carbon cycle uncertainty to future climate projection spread. *Tellus Series B-Chemical And Physical Meteorology,* **61**, 355-360.

Huntingford C, Cox PM, Mercado LM, Sitch S, Bellouin N, Boucher O, Gedney N (2011) Highly contrasting effects of different climate forcing agents on terrestrial ecosystem services. *Philosophical Transactions of the Royal Society A-Mathematical,Physical and*

Engineering Sciences, **369**, 2026-2037.

IPCC (2007), *Climate Change 2007. The Physical Science Basis: Summary for Policymakers*, Intergovernment Panel on Climate Change Secretariat, Geneva.

Iversen CM, Ledford J, Norby RJ (2008) CO2 enrichment increases carbon and nitrogen input from fine roots in a deciduous forest. *New Phytologist,* **179**, 837-847.

Jung M, Le Maire G, Zaehle S *et al.* (2007) Assessing the ability of three land ecosystem models to simulate gross carbon uptake of forests from boreal to Mediterranean climate in Europe. *Biogeosciences,* **4**, 647-656.

Jung M, Reichstein M, Margolis HA *et al.* (2011) Global patterns of land-atmosphere fluxes of carbon dioxide, latent heat, and sensible heat derived from eddy covariance, satellite, and meteorological observations. *Journal Of Geophysical Research,* **116**, G00J07, doi: 10.1029/2010jg001566.

Keeling CD, Whorf TP (2005) Atmospheric CO2 records from sites in the SIO sampling network. In: Trends: A Compendium of Data on Global Change. Carbon Dioxide Information Analysis Center, Oak Ridge National Laboratory, US Department of Energy, Oak Ridge, TN, USA. http://cdiac.ornl.gov/trends/co2/sio-mlo.htm

Krinner G, Viovy N, De Noblet-Ducoudré N *et al.* (2005) A dynamic global vegetation model for studies of the coupled atmosphere-biosphere system. *Global Biogeochemical Cycles,* **19**, GB1015, doi: 10.1029/2003gb002199.

Lasslop G, Reichstein M, Papale D *et al.* (2010) Separation of net ecosystem exchange into assimilation and respiration using a light response curve approach: critical issues and global evaluation. *Global Change Biology,* **16**, 187-208.

Lawrence D, Oleson KW, Flanner MG, Thorton PE, Swenson SC, Lawrence PJ, Zeng X, Yang Z-L, Levis S, Skaguchi K, Bonan GB, Slater AG (2011) Parameterization improvements and functional and structural advances in version 4 of the community land model. *Journal of Advances in Modeling Earth Systems,* **3**, doi:10.1029/2011ms000045.

Le Quere C, Raupach MR, Canadell JG *et al.* (2009) Trends in the sources and sinks of carbon dioxide. *Nature Geoscience,* **2**, 831-836.

Levy PE, Cannell MGR, Friend AD (2004) Modelling the impact of future changes in climate, CO2 concentration and land use on natural ecosystems and the terrestrial carbon sink.

Global Environmental Change, **14**, 21-30.

Long SP, Ainsworth EA, Leakey ADB, Nösberger J, Ort DR (2006) Food for Thought: Lower-Than-Expected Crop Yield Stimulation with Rising CO2 Concentrations. *Science,* **312**, 1918-1921.

Lu M, Zhou X, Luo Y, Fang C, Yang Q, Chen J, Yang X, Li B (2012) Responses of ecosystem carbon cycle to experimental warming: a meta-analysis. in preparation.

Lucht W, Prentice IC, Myneni RB *et al.* (2002) Climatic Control of the High-Latitude Vegetation Greening Trend and Pinatubo Effect. *Science,* **296**, 1687-1689.

Luo Y (2007) Terrestrial Carbon–Cycle Feedback to Climate Warming. *Annual Review of Ecology, Evolution, and Systematics,* **38**, 683-712.

Magnani F, Mencuccini M, Borghetti M *et al.* (2007) The human footprint in the carbon cycle of temperate and boreal forests. *Nature,* **447**, 848-850.

Matthews HD (2005) Decrease of emissions required to stabilize atmospheric CO2 due to positive carbon cycle-climate feedbacks. *Geophysical Research Letters,* **32**, L21707, doi:10.1029/2005GL023435.

Mcgrath GS, Sadler R, Fleming K, Tregoning P, Hinz C, Veneklaas EJ (2012) Tropical cyclones and the ecohydrology of Australia's recent continental-scale drought. *Geophysical Research Letters,* **39**, L03404, doi: 10.1029/2011gl050263.

Melillo JM, Steudler PA, Aber JD *et al.* (2002) Soil warming and carbon-cycle feedbacks to the climate system. *Science,* **298**, 2173-2176.

Moorcroft PR (2006) How close are we to a predictive science of the biosphere? *Trends in Ecology & Evolution,* **21**, 400-407.

Nepstad DC, Moutinho P, Dias-Filho MB *et al.* (2002) The effects of partial throughfall exclusion on canopy processes, aboveground production, and biogeochemistry of an Amazon forest. *Journal Of Geophysical Research,* **107**, 8085 doi: 10.1029/2001jd000360.

Nepstad D, Lefebvre P, Lopes Da Silva U *et al.* (2004) Amazon drought and its implications for forest flammability and tree growth: a basin-wide analysis. *Global Change Biology,* **10**, 704-717.

Norby RJ, Delucia EH, Gielen B *et al.* (2005) Forest response to elevated CO2 is conserved

across a broad range of productivity. *Proceedings of the National Academy of Sciences of the United States of America,* **102**, 18052-18056.

Oleson KW, Lawrence DM, Gordon B, Flanner MG, Kluzek E, Peter J, Levis S, Swenson SC, Thornton E, Feddema J (2010) Technical description of version 4.0 of the Community Land Model (CLM). NCAR/TN-478+STR.

Pan Y, Birdsey RA, Fang J *et al.* (2011) A Large and Persistent Carbon Sink in the World's Forests. *Science,* **333**, 988-993.

Phillips OL, Aragao LEOC, Lewis SL *et al.* (2009) Drought Sensitivity of the Amazon Rainforest. *Science,* **323**, 1344-1347.

Phillips OL, Van Der Heijden G, Lewis SL *et al.* (2010) Drought–mortality relationships for tropical forests. *New Phytologist,* **187**, 631-646.

Piao S, Friedlingstein P, Ciais P, Zhou L, Chen A (2006) Effect of climate and CO2 changes on the greening of the Northern Hemisphere over the past two decades. *Geophysical Research Letters,* **33**, L23402, doi:10.1029/2006gl028205.

Piao SL, Friedlingstein P, Ciais P, Viovy N, Demarty J (2007) Growing season extension and its impact on terrestrial carbon cycle in the Northern Hemisphere over the past 2 decades. *Global Biogeochemical Cycles,* **21**, doi:10.1029/2006gb002888.

Piao SL, Ciais P, Friedlingstein P *et al.* (2008) Net carbon dioxide losses of northern ecosystems in response to autumn warming. *Nature,* **451**, 49-53.

Piao S, Ciais P, Friedlingstein P, De Noblet-Ducoudré N, Cadule P, Viovy N, Wang T (2009) Spatiotemporal patterns of terrestrial carbon cycle during the 20th century. *Global Biogeochem. Cycles,* **23**, GB4026, doi:10.1029/2008gb003339.

Piao S, Friedlingstein P, Ciais P, Peylin P, Zhu B, Reichstein M (2009) Footprint of temperature changes in the temperate and boreal forest carbon balance. *Geophysical Research Letters,* **36**, L07404, doi:10.1029/2009gl037381.

Poulter B, Arag o L, Heyder U *et al.* (2010) Net biome production of the Amazon Basin in the 21st century. *Global Change Biology,* **16**, 2062-2075.

Poulter B, Frank DC, Hodson EL, Zimmermann NE (2011) Impacts of land cover and climate data selection on understanding terrestrial carbon dynamics and the CO2 airborne fraction. *Biogeosciences,* **8**, 2027-2036.

Randerson JT, Hoffman FM, Thornton PE *et al.* (2009) Systematic assessment of terrestrial biogeochemistry in coupled climate–carbon models. *Global Change Biology,* **15**, 2462-2484.

Richardson AD, Andy Black T, Ciais P *et al.* (2010) Influence of spring and autumn phenological transitions on forest ecosystem productivity. *Philosophical Transactions of the Royal Society B-Biological Sciences,* **365**, 3227-3246.

Scheffer M, Brovkin V, Cox PM (2006) Positive feedback between global warming and atmospheric CO2 concentration inferred from past climate change. *Geophysical Research Letters,* **33**, L10702, doi: 10.1029/2005gl025044.

Schimel DS, House JI, Hibbard KA *et al.* (2001) Recent patterns and mechanisms of carbon exchange by terrestrial ecosystems. *Nature,* **414**, 169-172.

Schwalm CR, Williams CA, Schaefer K *et al.* (2010) A model-data intercomparison of CO_2 exchange across North America: Results from the North American Carbon Program site synthesis. *Journal of Geophysical Research*, 115, G00H05, doi:10.1029/2009JG001229

Sitch S, Smith B, Prentice IC *et al.* (2003) Evaluation of ecosystem dynamics, plant geography and terrestrial carbon cycling in the LPJ dynamic global vegetation model. *Global Change Biology,* **9**, 161-185.

Sitch S, Huntingford C, Gedney N *et al.* (2008) Evaluation of the terrestrial carbon cycle, future plant geography and climate-carbon cycle feedbacks using five Dynamic Global Vegetation Models (DGVMs). *Global Change Biology,* **14**, 2015-2039.

Sitch S, et al. (2012) Trends and drivers of the regional-scale sources and sinks of carbon dioxide over the past two decades, in preparation

Smith B, Prentice IC, Sykes MT (2001) Representation of vegetation dynamics in the modelling of terrestrial ecosystems: comparing two contrasting approaches within European climate space. *Global Ecology And Biogeography,* **10**, 621-637.

Sokolov AP, Kicklighter DW, Melillo JM, Felzer BS, Schlosser CA, Cronin TW (2008) Consequences of Considering Carbon–Nitrogen Interactions on the Feedbacks between Climate and the Terrestrial Carbon Cycle. *Journal Of Climate,* **21**, 3776-3796.

Stephens BB, Gurney KR, Tans PP *et al.* (2007) Weak Northern and Strong Tropical Land Carbon Uptake from Vertical Profiles of Atmospheric CO2. *Science,* **316**, 1732-1735.

Stöckli R, Lawrence DM, Niu GY *et al.* (2008) Use of FLUXNET in the Community Land Model development. *Journal Of Geophysical Research,* **113**, G01025, doi: 10.1029/2007jg000562.

Thornton PE, Doney SC, Lindsay K *et al.* (2009) Carbon-nitrogen interactions regulate climate-carbon cycle feedbacks: results from an atmosphere-ocean general circulation model. *Biogeosciences,* **6**, 2099-2120.

Tribuzy, E. S. (2005), Variacoes da temperatura foliar do dossel e o seuefeito na taxa assimilatoria de CO2 na Amazonia Central, Ph.D. dissertation, Univ. de Sao Paulo, Sao Paulo.

Wang W, Wang W-J, Li J-S, Wu H, Xu C, Liu T (2010) The Impact of Sustained Drought on Vegetation Ecosystem in Southwest China Based on Remote Sensing. *Procedia Environmental Sciences,* **2**, 1679-1691.

Wang W, Ciais P, Nemani RR, *et al* (2012) Variations in atmospheric co2 growth rates controlled by tropical temperature. *Environmental Research Letters,* (submitted).

Wang X, Piao S, Ciais P, Li J, Friedlingstein P, Koven C, Chen A (2011) Spring temperature change and its implication in the change of vegetation growth in North America from 1982 to 2006. *Proceedings of the National Academy of Sciences,* **108**, 1240-1245.

Welp LR, Keeling RF, Meijer HaJ *et al.* (2011) Interannual variability in the oxygen isotopes of atmospheric CO2 driven by El Nino. *Nature,* **477**, 579-582.

Woodward FI, Smith TM, Emanuel WR (1995) A global land primary productivity and phytogeography model. *Global Biogeochemical Cycles,* **9**, 471-490.

Woodward FI, Lomas MR (2004) Simulating vegetation processes along the Kalahari transect. *Global Change Biology,* **10**, 383-392.

Zaehle S, Sitch S, Prentice IC *et al.* (2006) The importance of age-related decline in forest npp for modeling regional carbon balances. *Ecological Applications,* **16**, 1555-1574.

Zaehle S, Friend AD (2010) Carbon and nitrogen cycle dynamics in the O-CN land surface model: 1. Model description, site-scale evaluation, and sensitivity to parameter estimates. *Global Biogeochemical Cycles,* **24**, GB1005, doi:10.1029/2009gb003521.

Zaehle S, Dalmonech D (2011) Carbon–nitrogen interactions on land at global scales: current understanding in modelling climate biosphere feedbacks. *Current Opinion in*

Environmental Sustainability, **3**, 311-320.

Zeng N, Mariotti A, Wetzel P (2005) Terrestrial mechanisms of interannual CO2 variability. *Global Biogeochemical Cycles,* **19**, GB1016, doi:10.1029/2004gb002273.

Zeng N, Qian H, Roedenbeck C, Heimann M (2005) Impact of 1998-2002 midlatitude drought and warming on terrestrial ecosystem and the global carbon cycle. *Geophysical Research Letters,* **32**, doi:10.1029/2005gl024607.

Zhang X, Goldberg M, Tarpley D, Friedl MA, Morisette J, Kogan F, Yu Y (2010) Drought-induced vegetation stress in southwestern North America. *Environmental Research Letters,* **5**, 024008.

Zhao M, Running SW (2010) Drought-induced reduction in global terrestrial net primary production from 2000 through 2009. *Science,* **329**, 940-943.

Figure Legends

Figure 1. The magnitude of global Gross Primary Production (GPP) and global Net Biome Productivity (NBP) estimated by the 10 carbon cycle models. x-axis indicates mean annual global GPP during 1982-2008 with error bars showing standard deviation of the inter-annual variations. y-axis indicate mean annual global NBP during 1980-2009 with error bars showing standard deviation of the inter-annual variations. The red line shows global GPP estimated by a data driven model tree ensemble approach (JU11, Jung et al., 2011), while black lines shows global Residual Land Sink (RLS) (Friedlingstein et al., 2010). Global RLS is estimated as the difference between CO_2 emissions (from fossil fuel combustion and land use change) and carbon storage change in the atmosphere (atmospheric CO_2 growth rate) and in the oceans (model simulated ocean carbon sink) (Friedlingstein et al., 2010). The 10 carbon cycle models include Community Land Model 4C (CLM4C), Community Land Model 4CN (CLM4CN), HYLAND, Lund-Potsdam-Jena (LPJ), LPJ-GUESS, O-CN (OCN), ORCHIDEE, Sheffield-DGVM (SDGVM), TRIFFID and VEGAS.

Figure 2. Color-coded correlation matrixes for global GPP estimated by the 10 carbon cycle models and a data driven model tree ensemble approach (JU11, Jung et al., 2011) and global NBP estimated by the 10 carbon cycle models and global Residual Land Sink (RLS) (Friedlingstein et al., 2010). The correlation matrixes display (**a**) correlation coefficient in pairs among detrended GPP anomalies estimated by the different approaches during 1982-2008. (**b**) correlation coefficient in pairs among detrended NBP anomalies estimated by different models and RLS during 1980-2009. Model abbreviations are the same as in Figure 1.

Figure 3. The response of global Gross Primary Production (GPP), global Net Biome Production (NBP) and global Residual Land Sink (RLS) to (**a**) interannual variation in temperature (γ_{GPP}^{int} , γ_{NBP}^{int} and γ_{RLS}^{int} , respectively) and (**b**) interannual variation in precipitation (δ_{GPP}^{int} , δ_{NBP}^{int} and δ_{RLS}^{int} , respectively). γ_{GPP}^{int} and δ_{GPP}^{int} are estimated using Eq.1 with data during 1982-2008. γ_{NBP}^{int} , δ_{NBP}^{int} , γ_{RLS}^{int} , and δ_{RLS}^{int} estimated using Eq.1 with data

during 1980-2009. Grey area indicates the standard error of γ_{RLS}^{int} and δ_{RLS}^{int}. Error bars show standard error of the sensitivity estimates. Dashed error bars in both (a) and (b) indicate the estimated sensitivity from the regression approaches are statistically insignificant (P>0.05). The red line shows the 1σ range of β_{GPP} estimated by JU11's GPP products using Eq. 3. Model abbreviations are the same as in Figure 1.

Figure 4. Comparisons of observed relative response of Net Primary Production (NPP) to temperature change in warming experiments (Lu et al., in preparation, Table S1) and estimated relative response of NPP to interannual variation in temperature ($R\gamma_{NPP}^{int}$, the ratio of γ_{NPP}^{int} to 30 year average NPP) by 10 models for the period of 1980-2009. The gray histogram at each site shows the frequency distribution of $R\gamma_{NPP}^{int}$ according to the ensemble of 10 model simulations at the grid containing the experiment site and at model grids with grassland dominant land cover (grassland vegetation more than 50% according to GLC land cover map, changing the threshold of grassland percentage from 50% to 70% only induce small change in the frequency distribution of $R\gamma_{NPP}^{int}$ (Figure S11)) and with similar climate to the experiment site (the difference in mean annual temperature less than 1°C and difference in mean annual precipitation less than 50 mm). The mean of model estimated $R\gamma_{NPP}^{int}$ is shown in dashed black line. Model estimates at the gridcell of the experiment site are shown using model-specific mark and color with horizontal error bars showing standard error of $R\gamma_{NPP}^{int}$ estimated by the same model in the ensemble of this grid and grids with grassland dominant land cover and showing similar climate. The position of model-specific mark in the vertical axis only represents alphabetical order of model abbreviations. Observed relative temperature sensitivities of NPP in different plots or different time period in the same site, if reported, are shown separately in red circles. Since belowground NPP was not measured in HARS and Toolik Lake, experiment observed temperature sensitivities of NPP at the two sites were based on aboveground NPP measurements. The background color map shows spatial distribution of average of $R\gamma_{NPP}^{int}$ from 10 carbon cycle models. Pentagrams in the color map show locations

of experiment sites. Model abbreviations are the same as in Figure 1.

Figure 5. The response of global Gross Primary Production (GPP), global Net Biome Productivity (NBP) and global Residual Land Sink (RLS) to rising atmospheric CO_2 concentration (β_{GPP} , β_{NBP} and β_{RLS} , respectively). (**a**) β_{GPP} estimated by the two approaches. x-axis indicates β_{GPP} estimated by Eq. 2 using simulation S1, while y-axis indicates β_{GPP} estimated by Eq. 3 using simulation S2 with data during 1982-2008. (**b**) β_{NBP} estimated by two approaches. x-axis indicates β_{NBP} estimated by Eq. 2 using simulation S1, while y-axis indicates β_{NBP} estimated by Eq. 3 using simulation S2 with data during 1980-2009. Error bars show standard error of the sensitivity estimates. The solid black line shows β_{RLS} estimated by Eq. 3. Grey area shows the standard error of the β_{RLS} . Dashed error bars in both (a) and (b) indicate the estimated sensitivity from the regression approaches are statistically insignificant (P>0.05). Model abbreviations are the same as in Figure 1.

Figure 6. Comparison of the observed relative response of Net Primary Production (NPP) to rising atmospheric CO_2 concentration in the Free Atmospheric CO_2 Enrichment (FACE) experiment sites (Table S2) and estimated relative response of NPP to rising atmospheric CO_2 ($R\beta_{NPP}$, the ratio of β_{NPP} estimated by the Eq. 2 to 30 year average NPP) by 10 models for the period 1980-2009. The gray histogram at each site shows the frequency distribution of $R\beta_{NPP}$ according to the ensemble of 10 model simulations at the grid containing the experiment site and at model grids with forest dominant land cover (forest vegetation more than 50% according to GLC2000 land cover map, changing the threshold of forest percentage from 50% to 70% only induce small change in the frequency distribution of $R\beta_{NPP}$ (Figure S12)) and with similar climate to the experiment site (the difference in mean annual temperature less than 1°C and difference in mean annual precipitation less than 50 mm). The mean of the model estimated $R\beta_{NPP}$ is shown in dashed black line. Model estimates at the

grid containing the experiment site are shown using model-specific symbol and color with horizontal error bars showing standard error of the $R\beta_{NPP}$ estimated by the same model in the ensemble of this grid and grids with forest as the dominant land cover having similar climate. The position of model-specific mark in the vertical axis only represent alphabetical order of model abbreviations. Observed NPP response to rising atmospheric CO_2 at different year at the same site are shown separately in red circles. The background color map shows spatial distribution of $R\beta_{NPP}$ estimated from the average NPP of the 10 carbon cycle models. Solid pentagrams in the map show locations of the FACE forest sites. Model abbreviations are the same to Figure 1.

Figure 1

Figure 2

Figure 3

Figure 4

Figure 5

Figure 6

Figure Legends

Figure 1. The magnitude of global Gross Primary Production (GPP) and color-coded correlation matrix for global GPP estimated by the 10 carbon cycle models and a data driven model tree ensemble approach (JU11, Jung et al., 2011). (**a**) Mean annual global GPP during 1982-2008 with error bars showing standard deviation of the inter-annual variations. (**b**) The correlation matrix displays correlation coefficient in pairs among detrended GPP anomalies estimated by the different approaches during 1982-2008. The 10 carbon cycle models include Community Land Model 4C (CLM4C), Community Land Model 4CN (CLM4CN), HYLAND, Lund-Potsdam-Jena (LPJ), LPJ-GUESS, O-CN (OCN), ORCHIDEE, Sheffield-DGVM (SDGVM), TRIFFID and VEGAS.

Figure 2. The response of global Gross Primary Production (GPP) to interannual variation in temperature ($\gamma_{GPP}^{\text{int}}$), interannual variation in precipitation ($\delta_{GPP}^{\text{int}}$), and rising atmospheric CO_2 concentration (β_{GPP}) during 1982-2008. (**a**) $\gamma_{GPP}^{\text{int}}$ and $\delta_{GPP}^{\text{int}}$. $\gamma_{GPP}^{\text{int}}$ and $\delta_{GPP}^{\text{int}}$ are estimated using Eq.1 and simulation S2. Error bars show standard error of the sensitivity estimates. (**b**) β_{GPP} estimated by two approaches. x-axis indicates β_{GPP} estimated by Eq. 2 using simulation S1, while y-axis indicates β_{GPP} estimated by Eq. 3 using simulation S2. Error bars show standard error of the sensitivity estimates. The solid black line shows β_{GPP} estimated by JU11's GPP products using Eq. 3. The red line shows the 1σ range of β_{GPP} estimated by JU09's GPP products using Eq. 3. Dashed error bars in both (a) and (b) indicate the estimated sensitivity from the regression approaches are statistically insignificant ($P>0.05$).

Figure 3. Comparisons of observed relative response of Net Primary Production (NPP) to temperature change in warming experiments (Lu et al., in preparation, Table S1) and estimated relative response of NPP to interannual variation in temperature (, the ratio of to 30 year average NPP) by 10 models for the period of 1980-2009. The gray histogram at each site

shows the frequency distribution of according to the ensemble of 10 model simulations at the grid containing the experiment site and at model grids with grassland dominant land cover (grassland vegetation more than 50% according to GLC land cover map) and with similar climate to the experiment site (the difference in mean annual temperature less than 1^{o}C and difference in mean annual precipitation less than 50 mm). The mean of model estimated is shown in dashed black line. Model estimates at the gridcell of the experiment site are shown using model-specific mark and color with horizontal error bars showing standard error of estimated by the same model in the ensemble of this grid and grids with grassland dominant land cover and showing similar climate. The position of model-specific mark in the vertical axis only represents alphabetical order of model abbreviations. Observed relative temperature sensitivities of NPP in different plots or different time period in the same site, if reported, are shown separately in red circles. Since belowground NPP was not measured in HARS and Toolik Lake, experiment observed temperature sensitivities of NPP at the two sites were based on aboveground NPP measurements. The background color map shows spatial distribution of average of from 10 carbon cycle models. Pentagrams in the color map show locations of experiment sites. Model abbreviations are the same as in Figure 1..

Figure 4. Comparison of the observed relative response of Net Primary Production (NPP) to rising atmospheric CO_2 concentration in the Free Atmospheric CO_2 Enrichment (FACE) experiment sites (Table S2) and estimated relative response of NPP to rising atmospheric CO_2 (, the ratio of estimated by the Eq. 2 to 30 year average NPP) by 10 models for the period 1980-2009. The gray histogram at each site shows the frequency distribution of according to the ensemble of 10 model simulations at the grid containing the experiment site and at model grids with forest dominant land cover (forest vegetation more than 50% according to GLC2000 land cover map) and with similar climate to the experiment site (the difference in mean annual temperature less than 1^{o}C and difference in mean annual precipitation less than 50 mm). The mean of the model estimated is shown in dashed black line. Model estimates at the grid containing the experiment site are shown using model-specific symbol and color with horizontal error bars showing standard error of the estimated by the same model in the ensemble of this grid and grids with forest as the dominant land cover having similar climate.

The position of model-specific mark in the vertical axis only represent alphabetical order of model abbreviations. Observed NPP response to rising atmospheric CO_2 at different year at the same site are shown separately in red circles. The background color map shows spatial distribution of estimated from the average NPP of the 10 carbon cycle models. Solid pentagrams in the map show locations of the FACE forest sites. Model abbreviations are the same to Figure 1.

Figure 5. The magnitude of global Net Biome Productivity (NBP) and color-coded correlation matrix for global NBP estimated by the 10 carbon cycle models and global Residual Land Sink (RLS) (Friedlingstein et al., 2010). (**a**) Mean annual global NBP during 1980-2009 with error bars showing standard deviation of the inter-annual variations. (**b**) The correlation matrix displays correlation coefficient in pairs among detrended NBP anomalies estimated by different models and RLS during 1980-2009. Global RLS is estimated as the difference between CO_2 emissions (from fossil fuel combustion and land use change) and carbon storage change in the atmosphere (atmospheric CO_2 growth rate) and in the oceans (model simulated ocean carbon sink) (Friedlingstein et al., 2010). Model abbreviations are the same as in Figure 1.

Figure 6. The response of global Net Biome Productivity (NBP) and global Residual Land Sink (RLS) to interannual variation in temperature ($\gamma_{NBP}^{\text{int}}$ and $\gamma_{RLS}^{\text{int}}$, respectively), interannual variation in precipitation ($\delta_{NBP}^{\text{int}}$ and $\delta_{RLS}^{\text{int}}$, respectively), and rising atmospheric CO_2 concentration (β_{NBP} and β_{RLS}, respectively) during 1980-2009. (**a**) $\gamma_{NBP}^{\text{int}}$, $\delta_{NBP}^{\text{int}}$, $\gamma_{RLS}^{\text{int}}$, and $\delta_{RLS}^{\text{int}}$ estimated using Eq.1. Error bars show standard error of the sensitivity estimates. Grey area indicates the standard error of $\gamma_{RLS}^{\text{int}}$ and $\delta_{RLS}^{\text{int}}$. (**b**) β_{NBP} estimated by two approaches. x-axis indicates β_{NBP} estimated by Eq. 2 using simulation S1, while y-axis indicates β_{NBP} estimated by Eq. 3 using simulation S2. Error bars show standard error of the sensitivity estimates. The solid black line shows β_{RLS} estimated by Eq. 3. Grey area shows the standard

error of the β_{RLS}. Dashed error bars in both (a) and (b) indicate the estimated sensitivity from the regression approaches are statistically insignificant (P>0.05). Model abbreviations are the same as in Figure 1.

Figure 1.

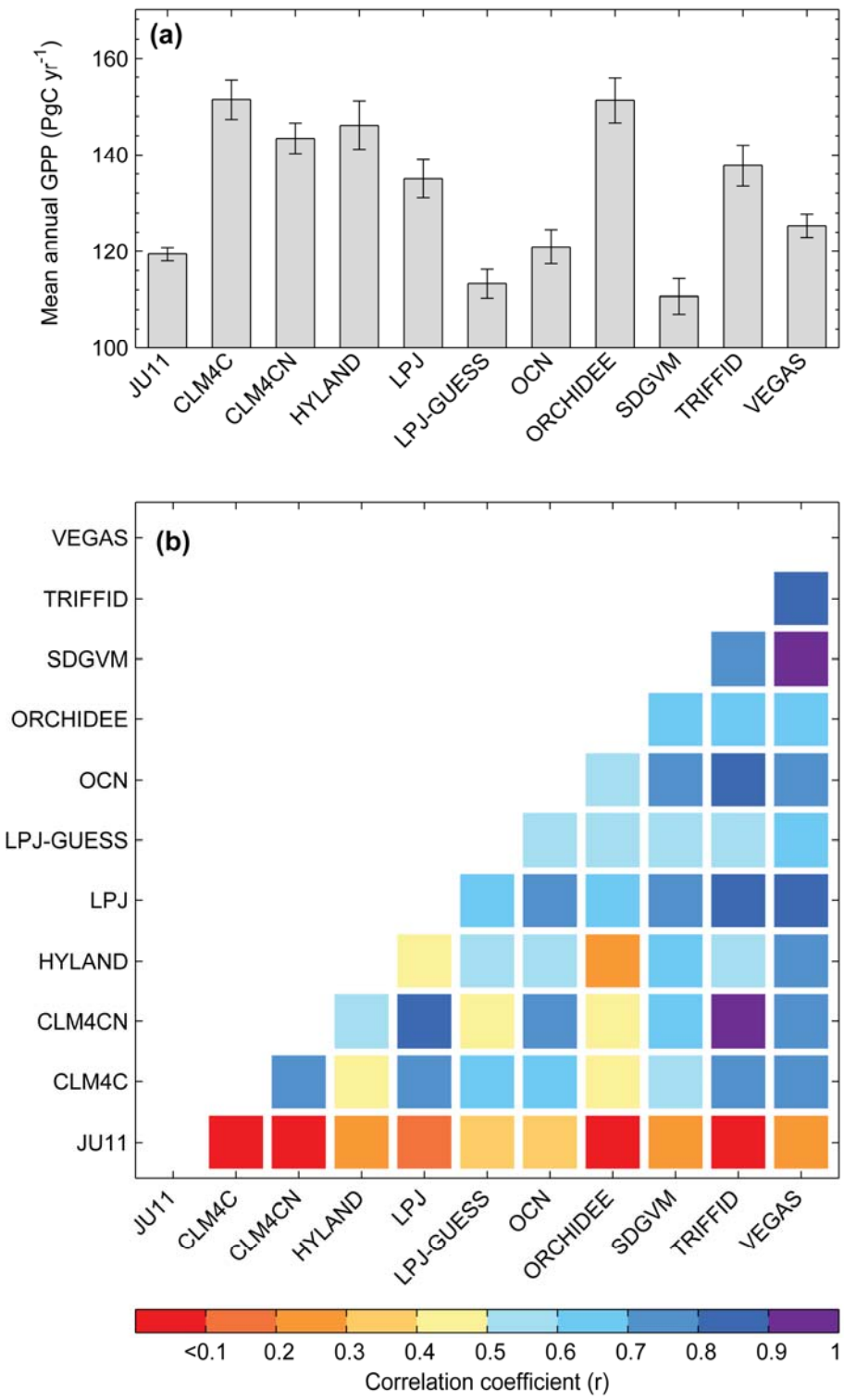
(a)
Mean annual GPP (PgC yr-1)
160
140
120
100
JU11
CLM4C
CLM4CN
HYLAND
LPJ
LPJ-GUESS
OCN
ORCHIDEE
SDGVM
TRIFFID
VEGAS
(b)
VEGAS
TRIFFID
SDGVM
ORCHIDEE
OCN
LPJ-GUESS
LPJ
HYLAND
CLM4CN
CLM4C
JU11
<0.1
0.2
0.3
0.4
0.5
0.6
0.7
0.8
0.9
1
Correlation coefficient (r)

Figure 2.

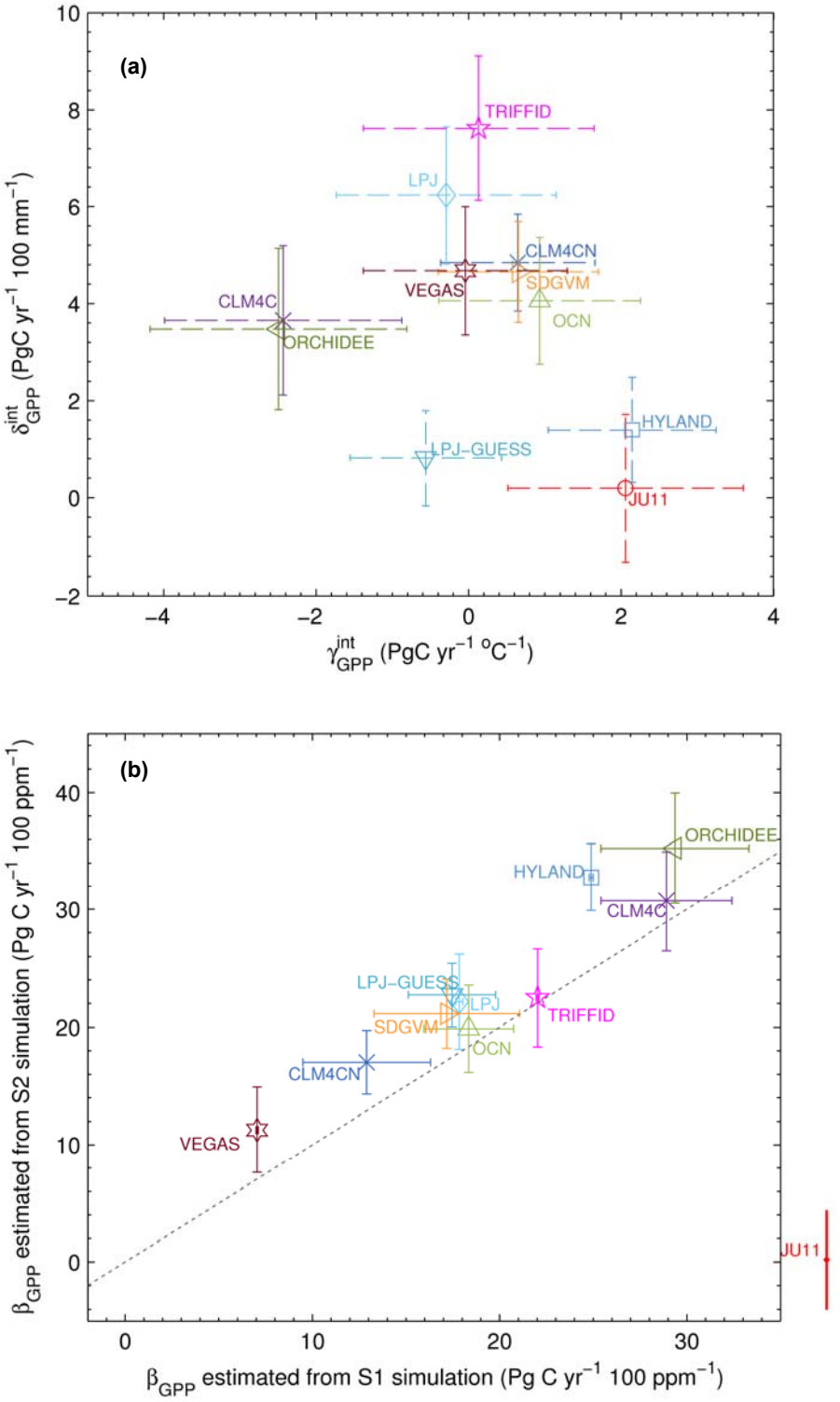
(a)
TRIFFID
LPJ
CLM4CN
VEGAS
SDGVM
CLM4C
OCN
ORCHIDEE
HYLAND
LPJ-GUESS
JU11
δ^{int}_{GPP} (PgC yr^{-1} 100 mm^{-1})
γ^{int}_{GPP} (PgC yr^{-1} °C^{-1})
(b)
ORCHIDEE
HYLAND
CLM4C
LPJ-GUESS
LPJ
TRIFFID
SDGVM
OCN
CLM4CN
VEGAS
JU11
β_{GPP} estimated from S2 simulation (Pg C yr^{-1} 100 ppm^{-1})
β_{GPP} estimated from S1 simulation (Pg C yr^{-1} 100 ppm^{-1})

Figure 3.

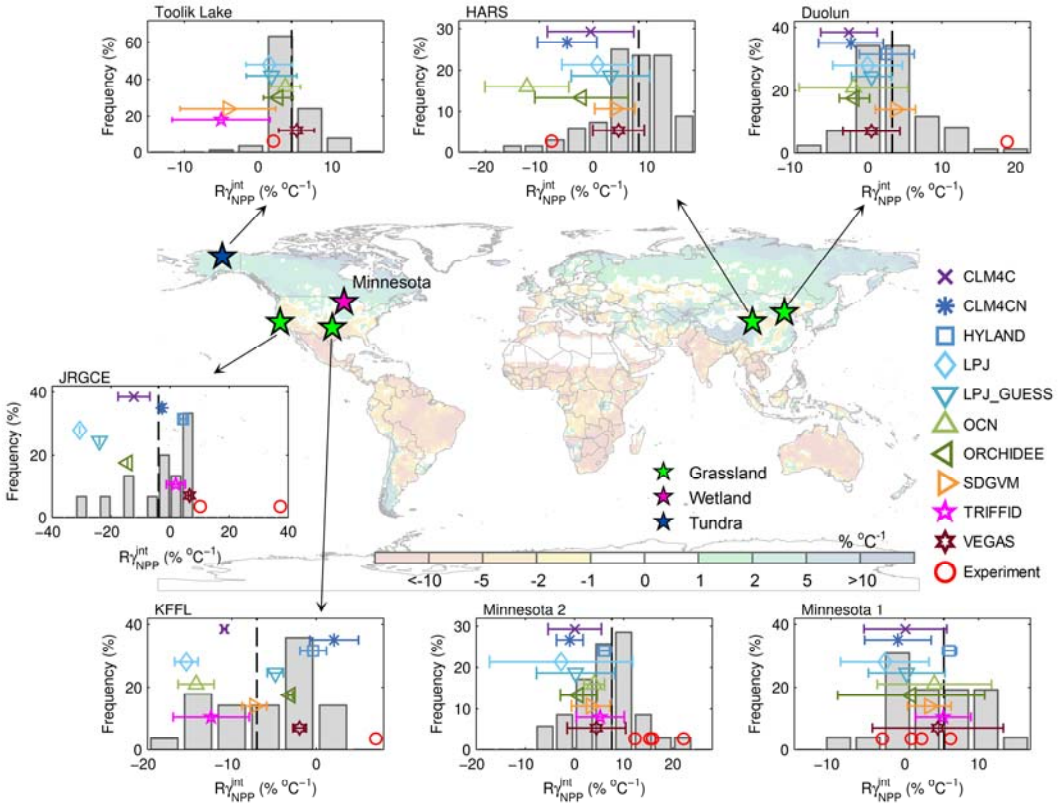
Toolik Lake
HARS
Duolun
JRGCE
KFFL
Minnesota 2
Minnesota 1
Minnesota
Frequency (%)
$R\gamma_{NPP}^{int}$ (% °C^{-1})
Grassland
Wetland
Tundra
% °C^{-1}
<-10 -5 -2 -1 0 1 2 5 >10
CLM4C
CLM4CN
HYLAND
LPJ
LPJ_GUESS
OCN
ORCHIDEE
SDGVM
TRIFFID
VEGAS
Experiment

Figure 4

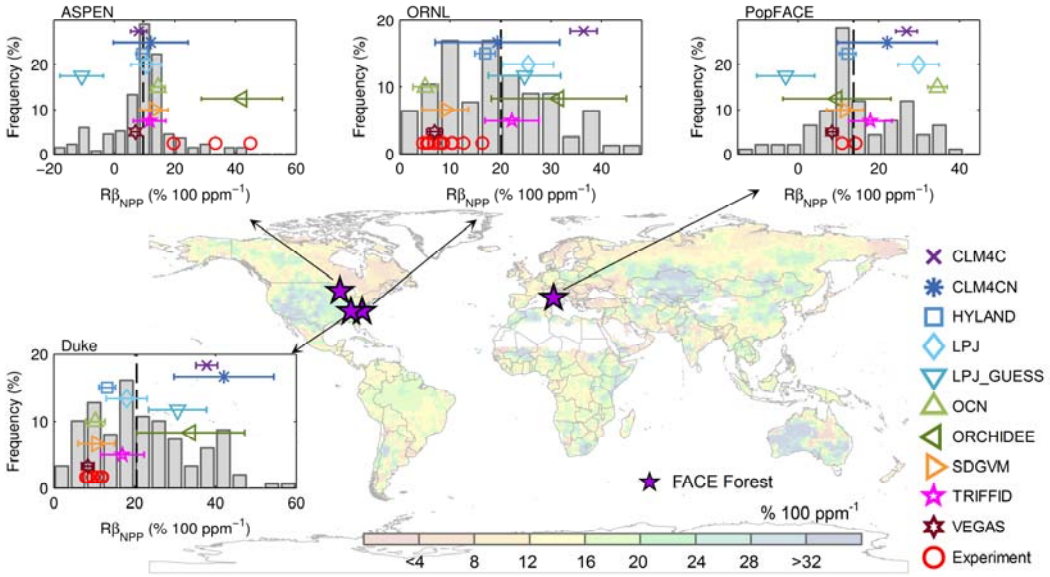
ASPEN
ORNL
PopFACE
Duke
Frequency (%)
Rβ$_{NPP}$ (% 100 ppm^{-1})
FACE Forest
% 100 ppm^{-1}
<4
8
12
16
20
24
28
>32
CLM4C
CLM4CN
HYLAND
LPJ
LPJ_GUESS
OCN
ORCHIDEE
SDGVM
TRIFFID
VEGAS
Experiment

Figure 5

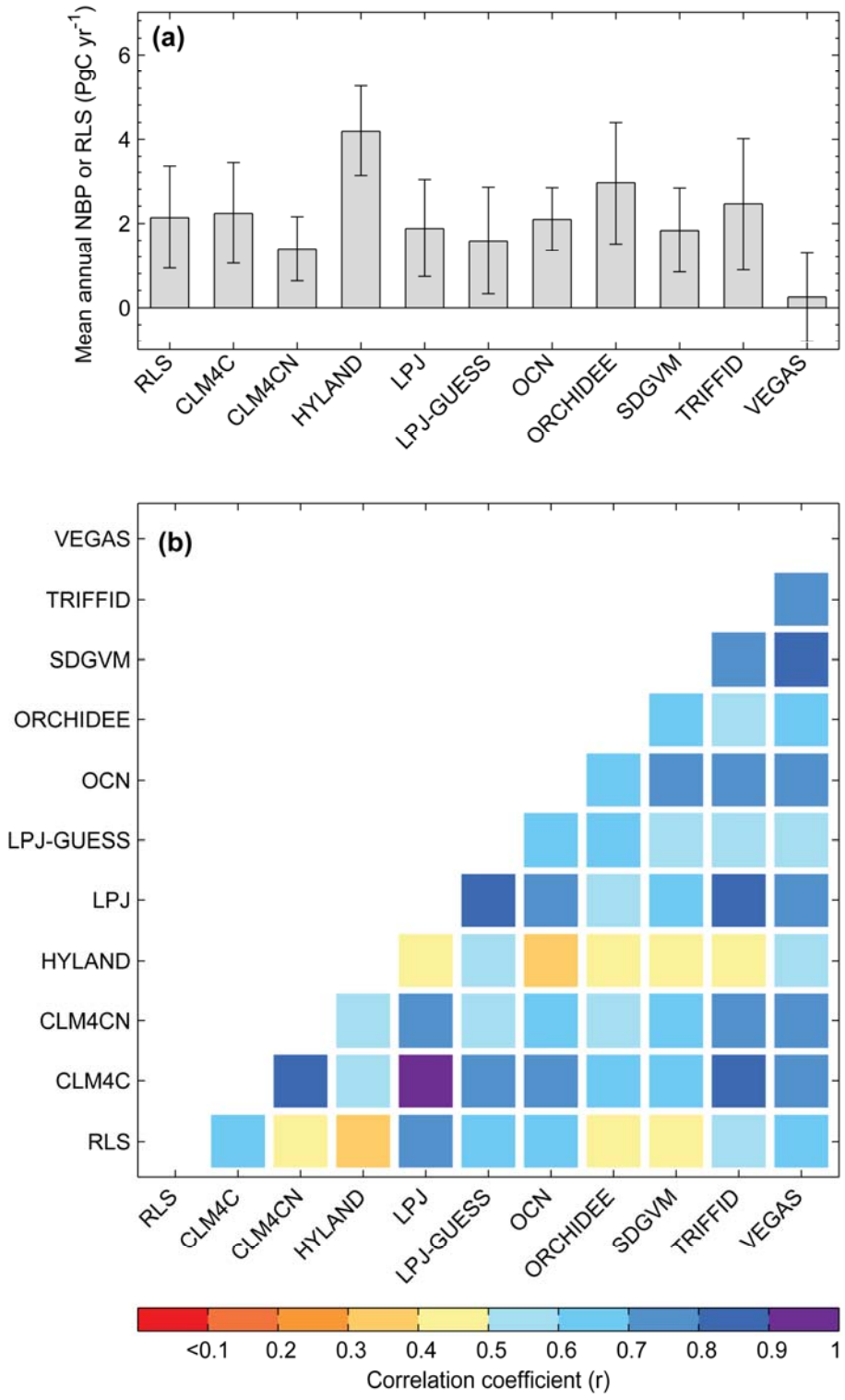
(a)
Mean annual NBP or RLS (PgC yr-1)
6
4
2
0
RLS
CLM4C
CLM4CN
HYLAND
LPJ
LPJ-GUESS
OCN
ORCHIDEE
SDGVM
TRIFFID
VEGAS
(b)
VEGAS
TRIFFID
SDGVM
ORCHIDEE
OCN
LPJ-GUESS
LPJ
HYLAND
CLM4CN
CLM4C
RLS
RLS
CLM4C
CLM4CN
HYLAND
LPJ
LPJ-GUESS
OCN
ORCHIDEE
SDGVM
TRIFFID
VEGAS
<0.1
0.2
0.3
0.4
0.5
0.6
0.7
0.8
0.9
1
Correlation coefficient (r)

Figure 6

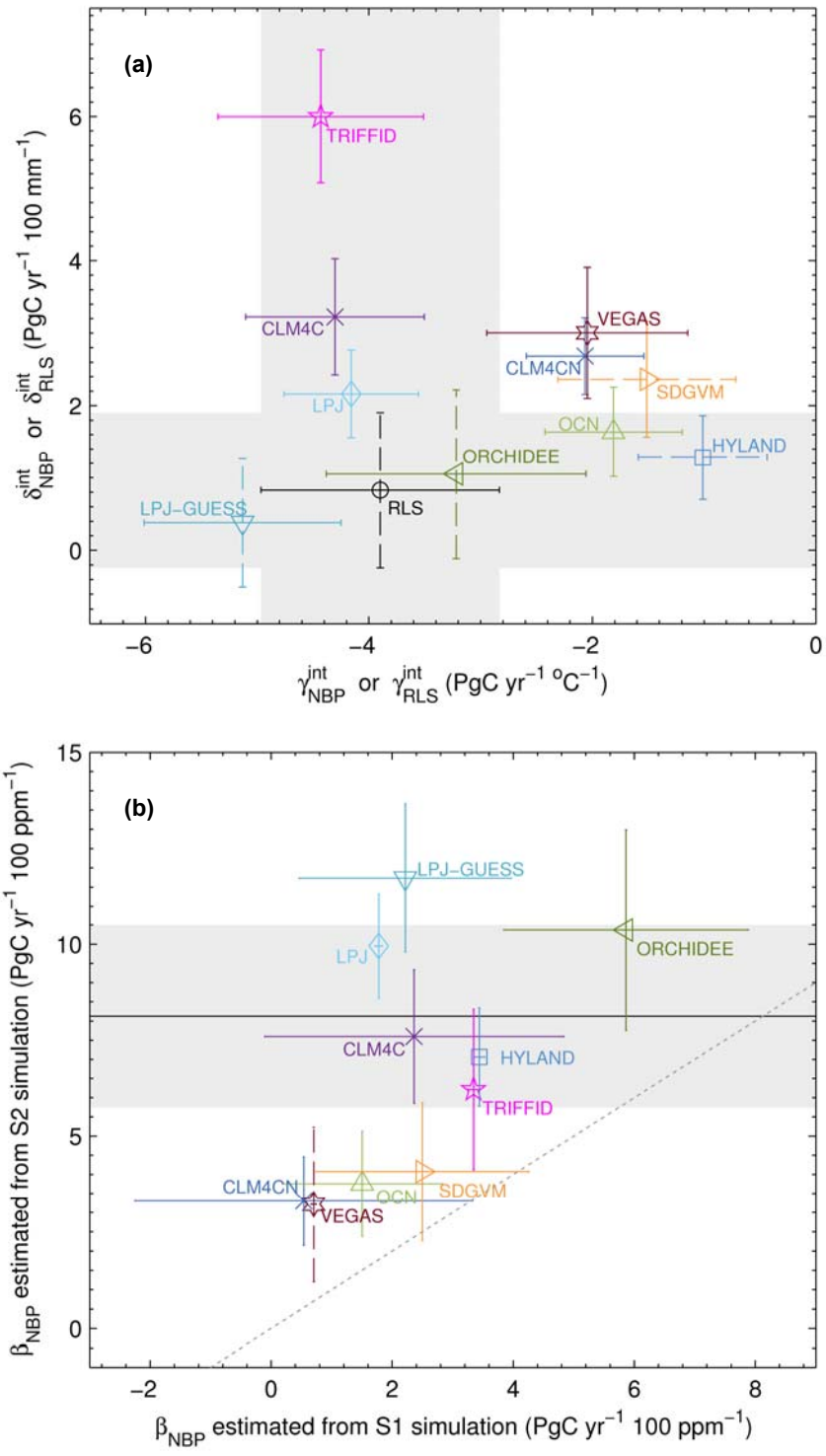
(a)
TRIFFID
CLM4C
VEGAS
CLM4CN
SDGVM
LPJ
OCN
HYLAND
ORCHIDEE
RLS
LPJ–GUESS
δ^{int}_{NBP} or δ^{int}_{RLS} (PgC yr^{-1} 100 mm^{-1})
γ^{int}_{NBP} or γ^{int}_{RLS} (PgC yr^{-1} °C^{-1})
(b)
LPJ–GUESS
ORCHIDEE
LPJ
CLM4C
HYLAND
TRIFFID
CLM4CN
OCN
SDGVM
VEGAS
β_{NBP} estimated from S2 simulation (PgC yr^{-1} 100 ppm^{-1})
β_{NBP} estimated from S1 simulation (PgC yr^{-1} 100 ppm^{-1})